In this study, genes regulated by AP2-O were first screened by comparison of gene expression between WT and *AP2-O* (–) parasites, and 15 genes were identified as being directly regulated by AP2-O. However, four genes reported so far were difficult to identify with this screening method. Of these genes, *P25* and *P28* were transcribed abundantly in female gametocytes (Paton *et al.*, 1993). Therefore, it seems that for these genes abundant transcripts had been synthesized in female gametocytes and masked the defect of transcription due to *AP2-O* disruption later in the ookinete stage. If so, many genes regulated by this TF could still remain to be identified.

In conclusion, our results demonstrate an AP2-related protein as a *Plasmodium* TF. At present, the *Plasmodium* AP2 family is the sole lineage-specific TF in *Plasmodium* spp. (Iyer *et al.*, 2008). Therefore, it is possible that these AP2 TFs participate in stage-specific gene regulations of *Plasmodium* spp. through their life cycle. Thus far, 26 AP2-related genes have been identified in the *Plasmodium* genome, but their roles in the life cycle, except for *AP2-O*, remain undefined. Further studies on AP2-related TFs are necessary to elucidate gene regulation mechanisms of *Plasmodium* parasites.

Experimental procedures

Parasite preparations

Female BALB/c mice infected (6–10 weeks old, Japan SLC, Hamamatsu, Japan) were prepared by peritoneal injection of *P. berghei* ANKA strain-infected blood that had been stored at –70°C. For ookinete culture, stored infected blood was injected intraperitoneally into mice that were made anaemic by phenyl-hydrazine treatment. After checking parasite exflagellation, infected blood was collected from the mice, passed through a CF11 column to deplete WBC, and diluted 10-fold with pH 8.0 RPMI1600 medium (Gibco, Gaithersburg, MD, USA), pH 8.0, containing 20% fetal calf serum and penicillin/streptomycin, and incubated at 20°C for 20–24 h. To prepare asexual-free gametocytes and ookinetes, infected anaemic mice were treated for 2 days with sulphadiazine (Sigma, St Louis, MO, USA) in their drinking water (10 μg ml^{-1}) to kill asexual stage parasites. Parasite infectivity in mosquitoes was evaluated as follows. When exflagellation rates were increased to over $20/10^5$ red blood cells, infected mice were subjected to bites of *Anopheles stephensi* mosquitoes. Fully engorged mosquitoes were selected and maintained at 20°C. After 2 week, the mosquitoes were dissected and the numbers of oocysts and sporozoites in their midguts were counted.

Cross-fertilization experiments

Cross-fertilization experiments were performed using a similar procedure to that described by Khan *et al.* (2005). *AP2-O* (–) parasites were fertilized with lines that have either defective male gametes (*P48/45*$^-$) or defective female gametes (*P47*$^-$). The numbers of unfertilized female gametes, deformed ookinetes and mature normal ookinetes were counted 20 h after fertilization, and conversion rates from female gametocytes to deformed ookinetes and mature normal ookinetes were calculated.

Genomic Southern hybridization

A 2 μg sample of *P. berghei* genomic DNA was digested with restriction enzymes, separated on a 1.5% agarose gel and transferred onto a nylon membrane. DNA fragments for Southern hybridization probes were amplified by PCR using genomic DNA as a template. The PCR primer pairs for AP2-O disruption were 5′-GCTGGAACTCCTTATTATGTTGCC-3′ and 5′-GCTTCAATCCACTATTTTCCAAACC-3′, and for the GFP-fused AP2-O-expressing mutants, the primers were 5′-GCTGGAACTCCTTATTATGTTGCC-3′ and 5′-GCT TCAATCCACTATTTTCCAAACC-3′. Amplified DNAs were labelled with alkaline phosphatase using AlkPhos Direct Labelling Reagents (Amersham Bioscience, Piscataway, NJ, USA) and subsequently detected using a CDP-Star chemiluminescent detection reagent (Amersham Bioscience).

Electrophoretic mobility shift assays (EMSA)

The *P. berghei* TF AP2 domain (amino acid residues 488–554) was produced as a glutathione S-transferase fusion protein using the GST Gene Fusion System with a pGEX 6p-1 vector (Amersham Bioscience). The AP2 domain coding region was amplified from *P. berghei* genomic DNA with the primer set: 5′-CGGGATCCGCCTTTAGGGTATTTGATGTAG AC-3′ and 5′-CCGCTCGAGTTAATACTTTAGTTTCATCATTT CGC-3′. The recombinant protein was purified with a glutathione Sepharose column (Amersham Bioscience). Longer probes were prepared by PCR with 5′-biotinylated primers using the cloned promoter region of *chitinase* or *SOAP* as templates. The primer pairs used were 5′-GGAGAGTTTT ATATTTTCAATTTTTATACTTAAAC-3′ and 5′-GAAAACGAA AAAAAGACAAATAAAAGAAC-3′ for *SOAP*, and 5′-ATTATT AATCACTATTTTATGGATGTAC-3′ and 5′-CCAAAAAATGG TGATATAGAAAAAGGC-3′ for the chitinase gene. Probes with a mutation in the TAGCTA sequence (TAGCTA to TAGGTA) were generated by PCR-mediated site-directed mutagenesis. Short oligonucleotide probes were prepared as follows. A synthetic 5′-biotinylated oligonucleotide was annealed with a complementary oligonucleotide to generate a double-strand probe. The oligonucleotide sequence was 5′-GTACATATTTTTTTGAATAGCTACCTTATTTTCCTTTGG-3′. Probes with various point mutations in the TAGCTA sequence were also prepared. EMSA was performed using a LightShift Chemiluminescence EMSA Kit (Pierce, Rockford, IL, USA). Briefly, GST-tagged protein (45 μg ml^{-1} final concentration) or GST as a control (30 μg ml^{-1} final concentration) was pre-incubated with a probe in EMSA buffer containing 50 ng μl^{-1} poly(dI-dC) for 20 min at room temperature. Gel electrophoresis was performed according to the manufacturer's protocol.

Targeted disruption of the AP2-O *gene*

The targeting vector was prepared by PCR according to Ecker *et al.* (2006). In brief, two fragments of the *AP2-O* gene were amplified by PCR using genomic DNA as the template with the primer pairs 5′-CGCGAGCTCGCAATATGGTATTA AATTTTGGGCTAGCCA-3′ (primer 1) and 5′-CGCGGATCC

GGTATTTTCATTGTGTTAAACGATATGTGA-3′ (primer 2), and 5′-CCGCTCGAGGTCCTATTTATCATTTTAAAATGTGT TTTATC-3′ (primer 3) and 5′-CGGGGTACCAATCGTCATA AATAGGAGTTATGAAGT-3′ (primer 4). The fragments were annealed to either side of the selectable marker gene (human DHFR) by PCR with primers 1 and 4. Gene targeting was performed as described previously (Yuda *et al.*, 1999a).

ChIP-quantitative PCR assays

ChIP was performed using a Chromatin Immunoprecipitation Assay Kit (Upstate Biotechnology, Lake Placid, NY, USA) according to the manufacturer's protocol. In brief, BALB/c mice (Japan SLC) were infected with malaria parasites expressing GFP-fused AP2-O (or WT parasites as a negative control) and treated with sulphadiazine to kill the parasite asexual stages. Blood was harvested and cultured to obtain ookinetes. After 20 h, each culture was fixed with 1% paraformaldehyde for 20 min at 30°C, washed with cold PBS, and incubated two or three times with NH_4Cl on ice for 30 min to lyse the erythrocytes. The ookinete-containing samples were sonicated in 250 µl of the lysis solution with a Bioruptor (Cosmo Bio, Tokyo, Japan) 10 times with a 30 s pulse and a 30 s interval. DNA fragmentation was checked by electrophoresis. IP was performed with anti-GFP polyclonal antibody (Clontech, Palo Alto, CA, USA) and pre-immune rabbit serum (negative control). DNA fragments obtained by IP were analysed by Real Time PCR using an iCycler iQ Real-Time Detection System (Bio-Rad, Hercules, CA, USA) with the primers listed in Table S5. Data were also presented as per cent input in Table S6.

Reporter assays with P. berghei *centromere plasmids*

Reporter assays were performed with the *P. berghei* centromere plasmid, Pcen (Fig. S3B). The upstream promoter region of the chitinase or SOAP gene (600 bp) was inserted into the EcoRV/BamHI site upstream of the GFP gene. This construct was transfected into cultured *P. berghei* shizonts by electroporation. Transfected parasites were selected by pyrimethamine to obtain parasites with the reporter construct. Ookinetes were cultured as described above and images were obtained with a fluorescent microscope equipped with a digital CCD camera system (Nikon, Kawasaki, Japan). Total fluorescent signal from each ookinete was analysed with Aqua Cosmos software (Hamamatsu Photonics, Hamamatsu, Japan). Background correction was performed by subtracting the intensity of a nearby cell-free region from the signal of the ookinete. Total of 30 ookinetes were used to determine promoter activity in each assay.

Construction of GFP-fused AP2-O-expressing parasites

GFP-fused AP2-O-expressing parasites (AP2-O::GFP) were constructed as follows. The targeted insertion vector was constructed in a pBluescript plasmid (Stratagene, La Jolla, CA, USA) (Fig. 1B). For the targeted insertion construct, a DNA fragment containing the 3′ part of the AP2-O coding region was amplified by PCR and inserted into the pBluescript XhoI/NheI site in frame with the GFP gene. The downstream region of the AP2-O gene was also amplified by PCR and inserted into the pBluescript BamHI/NotI site. Plasmids containing the construct were separated from plasmids without the construct by digestion with XhoI and NotI. AP2-O::GFP parasites were obtained by inserting the construct into the *AP2-O* locus by homologous recombination. Finally, AP2-O::GFP parasites were separated from WT by limiting dilution. GFP-fused protein fluorescence was observed with a microscope equipped with a filter set for GFP. For nuclear staining, Hoechst 34580 (Molecular Probes, Eugene, OR, USA) (0.02 µg ml^{-1} final concentration) was added to the medium, and the culture was incubated at room temperature for 10 min before fluorescence microscopy.

DNA microarray analysis

A custom 60-mer microarray (Agilent Technologies, Palo Alto, CA, USA) was designed based on *P. berghei* EST contigs (assembled from approximately 1×10^5 ESTs from different developmental stages, including blood stages, ookinetes, midgut sporozoites, salivary gland sporozoites and exoerythrocytic forms) and *P. berghei* genes in the NCBI Reference Sequence (RefSeq) Database (Pruitt *et al.*, 2007). This microarray contained approximately 21 000 probes and covered most *P. berghei* genes. Total RNA was prepared from malaria parasite blood stages and 12 h cultured ookinetes using RNAgents (Promega, Madison, WI, USA). Before RNA extraction, erythrocytes were lysed in 0.83% NH_4Cl. An RNA probe for one-colour analysis was synthesized using a Low RNA Fluorescent Linear Amplification Kit (Agilent Technologies) and fragmentated using a Gene Expression Hybridization Kit (Agilent Technologies) according to manufacturer's protocols. Hybridization was performed at 65°C. Three biologically independent experiments were performed in both *AP2-O* (–) and WT parasites. The data were analysed with Genespring software (Agilent Technologies). The data were normalized as follows. First, signal intensities less than 0.01 were set to 0.01. Then each chip was normalized to the 60th percentile of the measurements taken from the chip. Genes with significant differences between WT and *AP2-O* disruptants were selected by Student's *t*-test using *P*-value cut-off 0.05 (False discovery rate) and those whose expression was decreased at least fivefold in *AP2-O* (–) parasites were selected as candidates regulated by AP2-O. From the selected genes, those belonging to multigene families and those whose upstream sequences were not present in the *P. berghei* genome database were excluded. We have deposited the microarray data to Gene Expression Omnibus (GEO) DataSets with the Accession No. GSM359409–GSM359412, GSM359415 and GSM359428.

Quantitative RT-PCR

Quantitative analysis of *P. berghei AP2-O* expression was performed by quantitative RT-PCR. In brief, total RNA was extracted from asexual-free gametocytes and ookinetes. RT (1 µg of total RNA) was performed with random primers and Superscript II Reverse Transcriptase (Gibco BRL, Gaithersburg, MD, USA). SYBR Green PCR amplifications were performed using an iCycler iQ Real-Time Detection System (Bio-Rad Corporation) with the primer set: 5′-TTGGATT GCATCATGGTATG-3′ and 5′-TTCGGGGTTATTATTTTTAG GTTTTC-3′.

Identification of frequently occurring sequences in promoter regions

The frequency of occurrence of all possible 6 bp sequences in a gene's 1 kb upstream region was compared for the 15 genes in Fig. 2C and all annotated genes in the *P. berghei* genome (Table S2). Three 6 bp sequences, which had the five-base sequence TAGCT in common, were identified with significantly high frequencies (false discovery rate < 0.05) in the former group, and 10 of the 14 sequences with the highest frequency (false discovery rate < 0.5) could be aligned so that at least continuous 3 bp sequences overlap with each other. Based on the aligned sequences, the sequence conservation pattern in the 1 kb upstream regions of the 15 genes was generated using the fuzznuc and WebLogo programs (Olson, 2002; Crooks *et al.*, 2004).

Accession numbers

The PlasmoDB (http://www.plasmodb.org/plasmo/) accession number for *P. berghei AP2*-O is PB000572.01.0 and for *P. falciparum AP2*-O is PF11_0442. The reference numbers of blood-stage, ookinete and sporozoite ESTs are DC218765–DC224499, BB970378–BB981955, DC224500–DC235-241 respectively.

Acknowledgements

We thank N. Kimura for maintaining mosquito colonies. This work was supported by Ministry of Education, Science, Culture, and Sports of Japan (Grant 19041031, 19659105 and 20249023 to M.Y., and Grant 19041048 and 19790307 to S.I.). The research in the Leiden Malaria Research Group was supported by BioMalPar (EU).

References

Balaji, S., Babu, M.M., Iyer, L.M., and Aravind, L. (2005) Discovery of the principal specific transcription factors of Apicomplexa and their implication for the evolution of the AP2-integrase DNA binding domains. *Nucleic Acids Res* **33:** 3994–4006.

Bozdech, Z., Llinas, M., Pulliam, B.L., Wong, E.D., Zhu, J., and DeRisi, J.L. (2003) The transcriptome of the intraerythrocytic developmental cycle of *Plasmodium falciparum*. *PLoS Biol* **1:** E5.

Crooks, G.E., Hon, G., Chandonia, J.M., and Brenner, S.E. (2004) WebLogo: a sequence logo generator. *Genome Res* **14:** 1188–1190.

De Silva, E.K., Gehrke, A.R., Olszewski, K., Leon, I., Chahal, J.S., Bulyk, M.L., and Llinas, M. (2008) Specific DNA-binding by apicomplexan AP2 transcription factors. *Proc Natl Acad Sci USA* **105:** 8393–8398.

Dessens, J.T., Beetsma, A.L., Dimopoulos, G., Wengelnik, K., Crisanti, A., Kafatos, F.C., and Sinden, R.E. (1999) CTRP is essential for mosquito infection by malaria ookinetes. *EMBO J* **18:** 6221–6227.

Dessens, J.T., Siden-Kiamos, I., Mendoza, J., Mahairaki, V., Khater, E., Vlachou, D., *et al.* (2003) SOAP, a novel malaria ookinete protein involved in mosquito midgut invasion and oocyst development. *Mol Microbiol* **49:** 319–329.

Dubremetz, J.F., Garcia-Reguet, N., Conseil, V., and Fourmaux, M.N. (1998) Apical organelles and host-cell invasion by Apicomplexa. *Int J Parasitol* **28:** 1007–1013.

Ecker, A., Moon, R., Sinden, R.E., and Billker, O. (2006) Generation of gene targeting constructs for *Plasmodium berghei* by a PCR-based method amenable to high throughput applications. *Mol Biochem Parasitol* **145:** 265–268.

Ecker, A., Bushell, E.S., Tewari, R., and Sinden, R.E. (2008) Reverse genetics screen identifies six proteins important for malaria development in the mosquito. *Mol Microbiol* **70:** 209–220.

Gutterson, N., and Reuber, T.L. (2004) Regulation of disease resistance pathways by AP2/ERF transcription factors. *Curr Opin Plant Biol* **7:** 465–471.

Hall, N., Karras, M., Raine, J.D., Carlton, J.M., Kooij, T.W., Berriman, M., *et al.* (2005) A comprehensive survey of the *Plasmodium* life cycle by genomic, transcriptomic, and proteomic analyses. *Science (New York)* **307:** 82–86.

Ishino, T., Orito, Y., Chinzei, Y., and Yuda, M. (2006) A calcium-dependent protein kinase regulates *Plasmodium* ookinete access to the midgut epithelial cell. *Mol Microbiol* **59:** 1175–1184.

Iyer, L.M., Anantharaman, V., Wolf, M.Y., and Aravind, L. (2008) Comparative genomics of transcription factors and chromatin proteins in parasitic protists and other eukaryotes. *Int J Parasitol* **38:** 1–31.

Jofuku, K.D., den Boer, B.G., Van Montagu, M., and Okamuro, J.K. (1994) Control of *Arabidopsis* flower and seed development by the homeotic gene APETALA2. *Plant Cell* **6:** 1211–1225.

Kadota, K., Ishino, T., Matsuyama, T., Chinzei, Y., and Yuda, M. (2004) Essential role of membrane-attack protein in malarial transmission to mosquito host. *Proc Natl Acad Sci USA* **101:** 16310–16315.

Kaiser, K., Matuschewski, K., Camargo, N., Ross, J., and Kappe, S.H. (2004) Differential transcriptome profiling identifies *Plasmodium* genes encoding pre-erythrocytic stage-specific proteins. *Mol Microbiol* **51:** 1221–1232.

Khan, S.M., Franke-Fayard, B., Mair, G.R., Lasonder, E., Janse, C.J., Mann, M., and Waters, A.P. (2005) Proteome analysis of separated male and female gametocytes reveals novel sex-specific *Plasmodium* biology. *Cell* **121:** 675–687.

Le Roch, K.G., Zhou, Y., Blair, P.L., Grainger, M., Moch, J.K., Haynes, J.D., *et al.* (2003) Discovery of gene function by expression profiling of the malaria parasite life cycle. *Science (New York)* **301:** 1503–1508.

Mair, G.R., Braks, J.A., Garver, L.S., Wiegant, J.C., Hall, N., Dirks, R.W., *et al.* (2006) Regulation of sexual development of *Plasmodium* by translational repression. *Science (New York)* **313:** 667–669.

Olson, S.A. (2002) EMBOSS opens up sequence analysis. European Molecular Biology Open Software Suite. *Brief Bioinform* **3:** 87–91.

Paton, M.G., Barker, G.C., Matsuoka, H., Ramesar, J., Janse, C.J., Waters, A.P., and Sinden, R.E. (1993) Structure and expression of a post-transcriptionally regulated malaria gene encoding a surface protein from the sexual stages of *Plasmodium berghei*. *Mol Biochem Parasitol* **59:** 263–275.

Pruitt, K.D., Tatusova, T., and Maglott, D.R. (2007) NCBI

reference sequences (RefSeq): a curated non-redundant sequence database of genomes, transcripts and proteins. *Nucleic Acids Res* **35:** D61–D65.

Raibaud, A., Brahimi, K., Roth, C.W., Brey, P.T., and Faust, D.M. (2006) Differential gene expression in the ookinete stage of the malaria parasite *Plasmodium berghei*. *Mol Biochem Parasitol* **150:** 107–113.

Saul, A. (2007) Mosquito stage, transmission blocking vaccines for malaria. *Curr Opin Infect Dis* **20:** 476–481.

Tomas, A.M., Margos, G., Dimopoulos, G., van Lin, L.H., de Koning-Ward, T.F., Sinha, R., *et al.* (2001) P25 and P28 proteins of the malaria ookinete surface have multiple and partially redundant functions. *EMBO J* **20:** 3975–3983.

Vinetz, J.M., Valenzuela, J.G., Specht, C.A., Aravind, L., Langer, R.C., Ribeiro, J.M., and Kaslow, D.C. (2000) Chitinases of the avian malaria parasite *Plasmodium gallinaceum*, a class of enzymes necessary for parasite invasion of the mosquito midgut. *J Biol Chem* **275:** 10331–10341.

Vlachou, D., Schlegelmilch, T., Runn, E., Mendes, A., and Kafatos, F.C. (2006) The developmental migration of *Plasmodium* in mosquitoes. *Curr Opin Genet Dev* **16:** 384–391.

Young, J.A., Johnson, J.R., Benner, C., Yan, S.F., Chen, K., Le Roch, K.G., *et al.* (2008) In silico discovery of transcription regulatory elements in Plasmodium falciparum. *BMC Genomics* **9:** 70.

Yuda, M., and Ishino, T. (2004) Liver invasion by malarial parasites – how do malarial parasites break through the host barrier? *Cell Microbiol* **6:** 1119–1125.

Yuda, M., Sakaida, H., and Chinzei, Y. (1999a) Targeted disruption of the plasmodium berghei CTRP gene reveals its essential role in malaria infection of the vector mosquito. *J Exp Med* **190:** 1711–1716.

Yuda, M., Sawai, T., and Chinzei, Y. (1999b) Structure and expression of an adhesive protein-like molecule of mosquito invasive-stage malarial parasite. *J Exp Med* **189:** 1947–1952.

Yuda, M., Yano, K., Tsuboi, T., Torii, M., and Chinzei, Y. (2001) von Willebrand Factor A domain-related protein, a novel microneme protein of the malaria ookinete highly conserved throughout *Plasmodium* parasites. *Mol Biochem Parasitol* **116:** 65–72.

Supporting information

Additional supporting information may be found in the online version of this article.

Please note: Wiley-Blackwell are not responsible for the content or functionality of any supporting materials supplied by the authors. Any queries (other than missing material) should be directed to the corresponding author for the article.

Cellular Microbiology (2009) 11(9), 1329–1339
doi:10.1111/j.1462-5822.2009.01333.x
First published online 26 May 2009

LISP1 is important for the egress of *Plasmodium berghei* parasites from liver cells

Tomoko Ishino,[1†§] Bertrand Boisson,[1‡§] Yuki Orito,[2] Céline Lacroix,[1] Emmanuel Bischoff,[3] Céline Loussert,[4] Chris Janse,[5] Robert Ménard,[1] Masao Yuda[2] and Patricia Baldacci[1*]**

[1]*Institut Pasteur, Biologie et Génétique du Paludisme, 75724 Paris cedex 15, France.*
[2]*Department of Medical Zoology, Mie University School of Medecine, Mie 514-0001, Japan.*
[3]*Institut Pasteur, Plateforme Puces à ADN Génopole, Paris, France.*
[4]*Institut Pasteur, Plateforme de Microscopie Ultrastructurale, Paris, France.*
[5]*Department of Parasitology, Leiden University Medical Centre, Leiden, the Netherlands.*

Summary

Most Apicomplexa are obligatory intracellular parasites that multiply inside a so-called parasitophorous vacuole (PV) formed upon parasite entry into the host cell. *Plasmodium*, the agent of malaria and the Apicomplexa most deadly to humans, multiplies in both hepatocytes and erythrocytes in the mammalian host. Although much has been learned on how Apicomplexa parasites invade host cells inside a PV, little is known of how they rupture the PV membrane and egress host cells. Here, we characterize a *Plasmodium* protein, called LISP1 (liver-specific protein 1), which is specifically involved in parasite egress from hepatocytes. LISP1 is expressed late during parasite development inside hepatocytes and locates at the PV membrane. Intracellular parasites deficient in LISP1 develop into hepatic merozoites, which display normal infectivity to erythrocytes. However, LISP1-deficient liver-stage parasites do not rupture the membrane of the PV and remain trapped inside hepatocytes. LISP1 is the first *Plasmodium* protein shown by gene targeting to be involved in the lysis of the PV membrane.

Received 23 January, 2009; revised 27 April, 2009; accepted 29 April, 2009. For correspondence. *E-mail baldacci@pasteur.fr; Tel. (+33) 1 44 38 94 59; Fax (+33) 1 40 61 30 89; **E-mail m-yuda@doc.medic.mie-u.ac.jp; Tel. (+81) 59 231 5430; Fax (+81) 59 231 5430. Present addresses: †Department of Molecular Parasitology, Ehime University Graduate School of Medicine, Shitsukawa, Toon, Ehime 791-0295, Japan; ‡Laboratory of Human Genetics of Infectious Diseases, Rockefeller University, New York, NY 10065, USA. §These authors contributed equally to this work.

Introduction

Plasmodium, the agent of malaria, is an Apicomplexan parasite that cycles through a mosquito and a mammalian host. In the mammalian host, it multiplies by schizogony inside hepatocytes and erythrocytes. The parasite form inoculated by the mosquito, the sporozoite, invades hepatocytes where it transforms into thousands of merozoites, which in turn invade erythrocytes. The successive cycles of merozoite multiplication inside erythrocytes then cause the disease pathology (Miller *et al.*, 2002a,b).

The two cell invasive stages of *Plasmodium*, the sporozoite and the merozoite, differentiate intracellularly within a parasitophorous vacuole (PV). The PV membrane (PVM), which is formed upon zoite entry and is mainly derived from the host cell plasma membrane, is devoid of host cell integral proteins and thus prevents PV fusion to endosomal compartments (Lingelbach and Joiner, 1998; Bano *et al.*, 2007). The PVM thus provides a safe niche for the maturing parasite and allows passage of vital nutrients and signals via channels and transporters (see review Charpian and Przyborski, 2008). Among the parasite proteins known to be present in the PVM of infected erythrocytes are exported protein 1 (EXP1) (Simmons *et al.*, 1987) and several members of the early transcribed membrane proteins (ETRAMP) family, which are integral PVM proteins organized in oligomeric arrays (Spielmann *et al.*, 2006). In hepatocytes, the PVM also contains EXP1 (Doolan *et al.*, 1996) and the stage-specific ETRAMPs known as UIS3 and UIS4 (Matuschewski *et al.*, 2002). The latter two proteins are expressed in sporozoites and early liver stages (LS) and are essential for their growth (Mueller *et al.*, 2005a,b; Tarun *et al.*, 2007).

Once the parasite has multiplied inside the PV, how the progeny exits the PV and the host cell remains largely unknown (Blackman, 2008). Electron (Aikawa, 1971) and live (Wickham *et al.*, 2003) microscopy have provided evidence for two distinct stages in the release of merozoites from erythrocytes, with the successive rupture of the

PVM and of the erythrocyte membrane. The two-step model applies to the release of merozoites from hepatocytes (Meis and Verhave, 1988; Sturm *et al.*, 2006; 2009). After disruption of the PVM, merozoite-filled membrane-bound extrusions, called merosomes (Sturm *et al.*, 2006; 2009; Baer *et al.*, 2007; Thiberge *et al.*, 2007), detach from the infected hepatocyte before releasing free merozoites into the blood circulation.

Here, we identify and characterize a *Plasmodium* protein, called LISP1 (liver-specific protein 1), which is specifically expressed by the LS and is expressed at high levels late during its development. Inactivation of *Lisp1* in *Plasmodium berghei* indicates that LISP1 is important for the destruction of the PVM surrounding the LS.

Results

Identification of Lisp1

We previously constructed expressed sequence tag (EST) libraries from various stages of *P. berghei* ANKA parasites, including ookinetes, midgut sporozoites, salivary gland sporozoites, LS isolated from a rat liver 31 h post infection with sporozoites, and merozoites. *Lisp1* was identified as a transcript present only in the LS library and it aligned to four annotated *P. berghei* genes: PB000708.00.0, PB001247.00.0, PB000682.00.0 and PB000250.00.0. An independent *in silico* analysis also selected PB000708.00.0 and PB000682.00.0 as candidate liver-specific genes and real-time PCR analysis confirmed that they were highly expressed in LS. The *Lisp1* transcript is predicted to encode a protein of 3249 amino acids (Accession No. AB231328) with a signal peptide sequence and a potential EF-hand but no other recognizable functional domain (http://www.plasmodb.org). The *Plasmodium yoelii Lisp1* orthologue (PY04499) has recently been detected in a proteomic analysis of infected hepatocytes (Tarun *et al.*, 2008). Orthologues of *P. berghei Lisp1* are also found in *Plasmodium falciparum* (PF14_0179) and *Plasmodium vivax* (PVX_085550), but not in other Apicomplexa parasites such as *Cryptosporidium hominis*, *Toxoplasma gondii*, *Theileria annulata* or *Eimeria tenella.*

Lisp1 *is expressed specifically in LS*

To confirm the LS-specific expression of *Lisp1*, real-time PCR analysis was performed on RNA isolated from NK65 blood stages and salivary gland sporozoites, as well as infected HepG2 cells at different time points (Fig. 1A). *Lisp1* messenger RNA (mRNA) was barely detectable in blood stages, present at low levels in sporozoites, and its quantity increased dramatically during parasite development in HepG2 cells with a peak at 40 h (10^4-fold increase compared with blood stages). Similar results were obtained with RNA isolated from the liver of rats infected with *P. berghei* ANKA, with *Lisp1* expression peaking at 48 h (Fig. S1). Thus *Lisp1* appeared to be most highly expressed at late stages of intrahepatocytic parasite development, when merozoites are formed.

Next, the subcellular localization of LISP1 was addressed by immunofluorescence analysis (IFA) with an anti-LISP1 polyclonal antibody. While no signal was detected in midgut or salivary gland sporozoites (not shown) or purified blood-stage schizonts, parasites developing in the liver of rat 48 h after sporozoite inoculation were brightly stained (Fig. 1B). LISP1 was also detected in infected HepG2 cells at 36, 48 and 65 h post infection (Fig. 1C) where it appeared to be associated with the PVM surrounding the developing LS. To better define the localization of LISP1, IFA was performed with anti-LISP1 and anti-EXP1 antibodies. As shown in Fig. 1D, the two proteins colocalized confirming that LISP1 is present in the PVM and in agreement with the localization of PY04499 in *P. yoelii*-infected hepatocytes (Tarun *et al.*, 2008).

LISP1-deficient parasites have a decreased infectivity to the mammalian host

To address the *in vivo* function of LISP1, we inactivated the gene in both wild-type (WT) ANKA and NK65 strains of *P. berghei* by double-cross-over recombination. The endogenous *Lisp1* was either interrupted by the selectable marker (*Lisp1I*) (Fig. 2A) or replaced by the marker (*Lisp1*Δ) (Fig. 2B). The *Lisp1I* modification was introduced in the WT ANKA strain, generating clone Lisp1I. The *Lisp1*Δ modification was introduced in WT NK65, generating the clone NK65Lisp1Δ, and in an ANKA strain expressing green fluorescent protein (GFP) (Janse *et al.*, 2006a), generating clone Lisp1ΔGreen. Southern blot analysis confirmed the expected structure of all recombinant loci (Fig. S2). The absence of LISP1 protein in Lisp1ΔGreen parasites was confirmed by IFA of infected HepG2 cells with an anti-LISP1 antibody (Fig. 2C). Using the same antibody, Western blot analysis of extracts from HepG2 cells 48 h post infection with WT ANKA sporozoites detected the expected 380 kDa band, whereas no band was observed upon infection with Lisp1Δ parasites (Fig. 2D).

All the *Lisp1* mutant parasite clones displayed similar growth rates in mouse blood stages and similar infectivity in mosquitoes, and yielded similar numbers of salivary gland sporozoites when compared with WT parasites (not shown). This indicated that *Lisp1* has no essential role in erythrocytic and mosquito stages. The infectivity of mutant sporozoites was measured by checking the emergence of blood-stage parasites in rats injected intravenously with Lisp1I salivary gland sporozoites. The parasitaemias

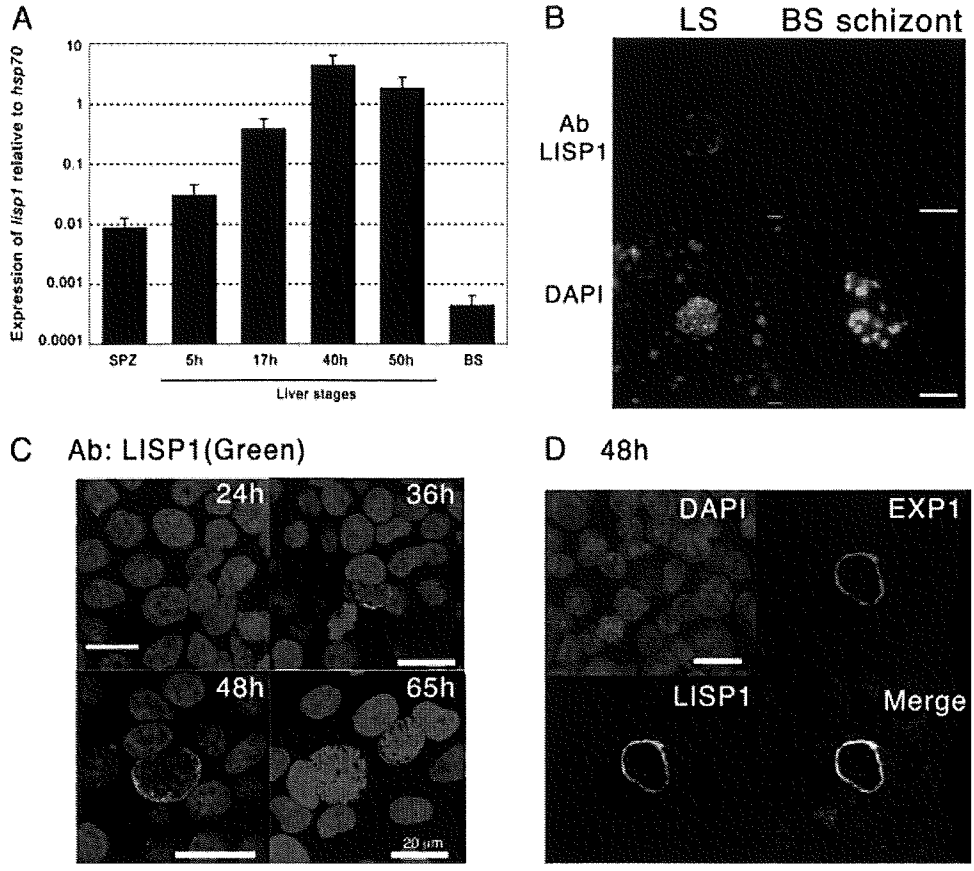

Fig. 1. *Pblisp1* is specifically expressed in late liver stages and localizes to the PVM.
A. Histogram representation of real-time RT-PCR analysis of *lisp1* relative gene expression in *P. berghei* sporozoites (SPZ), HepG2 cells 5, 17, 40 and 50 h post infection and mixed blood stages (BS). The value was normalized to the expression of *hsp70* mRNA in each sample. Error bars are standard deviation.
B. Immunofluorescence analysis of frozen sections of rat liver 48 h post infection (LS) and purified BS schizonts. Samples were incubated with an anti-LISP1 antibody followed by FITC-conjugated secondary antibody and nuclei were stained with DAPI (scale bar 5 µm).
C. Micrograph of confocal section of LS. HepG2 cells were fixed at 24, 36, 48 and 65 h post infection with WT ANKA sporozoites, incubated with an anti-LISP1 antibody followed by Alexa 488-conjugated secondary antibody and nuclei stained with DAPI (scale bars 20 µm).
D. Micrograph of confocal section of LS. HepG2 cells were fixed 48 h post infection with WT ANKA sporozoites, incubated with anti-LISP1 and anti-EXP1 antibodies followed by Alexa 488-conjugated secondary antibodies and nuclei stained with DAPI (scale bar 20 µm).

obtained with mutant sporozoites were significantly different ($P = 1.4 \times 10^{-7}$) from those obtained with WT sporozoites (Fig. 2E) and indicated a 15-fold decrease in infectivity. Similar results were obtained with all *Lisp1* mutants (Fig. S3), so the two ANKA-derived mutants, Lisp1l and Lisp1ΔGreen, were used for further analysis.

Mutant LS parasites are impaired in merozoite release

We then examined the intrahepatocytic development of mutant parasites. First, 300 000 ANKA or Lisp1l sporozoites were injected intravenously into rats and 48 h later the number of LS were counted in liver sections immunostained with anti-CS antibodies. No significant difference was observed between the numbers of ANKA and Lisp1l LS parasites (Fig. 3A). Second, the development of WT and Lisp1ΔGreen LS was assessed with an anti-UIS4 antibody. The presence of a PVM was detected until 48 h in both WT and mutant parasites (Fig. 3B). Furthermore, when WT and Lisp1l (or Lisp1ΔGreen) sporozoites were incubated with HepG2 cells there was no significant difference in the number of LS parasites at 48 or 64 h (data not shown). Finally, we assessed by real-time imaging the development of WT and mutant LS at 24, 36 and 48 h post infection of HepG2 cells. Again there was no significant difference in the size of WT compared with mutant LS over this period (Fig. S4).

To examine hepatic merozoite development, the numbers of merozoites released from HepG2 cells 65 h post infection were compared between the WT and mutant parasites. To internally control experiments, mixed infections were performed with a 1:1 ratio of sporozoites of Lisp1ΔGreen and of WTRed, a WT ANKA derivative that expresses red fluorescent protein (RFP) from the

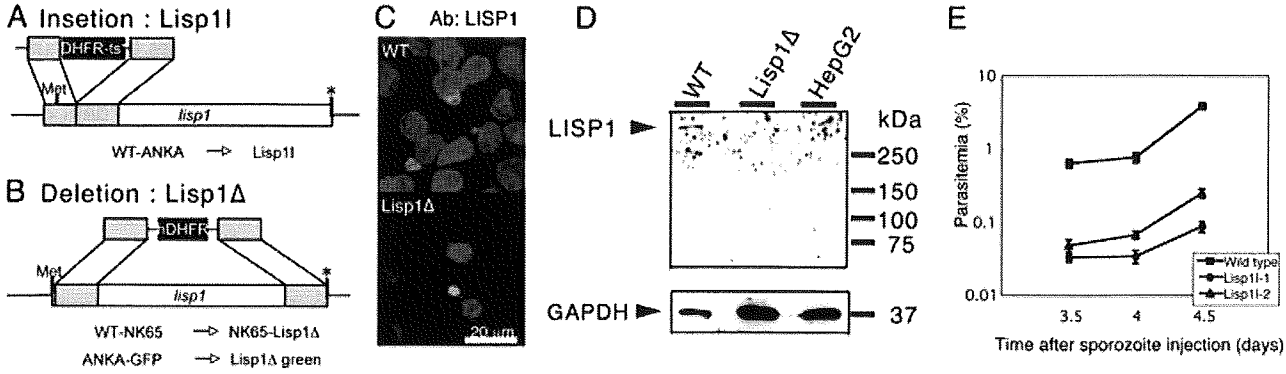

Fig. 2. Targeted gene disruption of *lisp1*.
A. Schematic representation of *Lisp1l* gene disruption.
B. Schema of *Lisp1Δ* gene disruption. Shaded boxes indicate the regions of homology used for double-cross-over recombination; black boxes indicate the selectable marker; Met and the asterisk (*) indicate the initiation and stop codons respectively.
C. Absence of LISP1 protein in Lisp1Δ parasites. Microscopy image of HepG2 cells 48 h post infection with WTGreen or Lisp1ΔGreen. LS were labelled with anti-LISP1 antibody and Alexa 647-conjugated secondary antibody (red); nuclei stained with DAPI (blue).
D. Western blot analysis of extracts of HepG2 cells 48 h post infection with ANKA (WT) or Lisp1ΔGreen sporozoites. Arrowheads indicate the bands of LISP1 and human GAPDH.
E. Lisp1l sporozoites have a decreased infectivity in the mammalian host. A total of 30 000 wild-type or Lisp1l sporozoites, from two independent Lisp1l clones, were injected intravenously into rats and blood parasitaemias were examined by Geimsa staining. The error bars show the standard errors from three rats.

eef1α promoter (Sturm *et al.*, 2009) and the ratio of green versus red merozoites (G/R) released in the culture supernatant was calculated (see Table 1). To verify that green and red merozoites were detected with similar efficiency, cells were co-infected with a 1:1 ratio of WTGreen and WTRed sporozoites. An average G/R merozoite ratio of 1 was found, confirming that green- and red-fluorescent merozoites were detected with similar efficiency. In contrast, co-infections with Lisp1ΔGreen and WTRed parasites gave an average G/R merozoite ratio of 0.1:1. The 10-fold reduction in the number of merozoites released by mutant LS suggested that LISP1 might be important for merozoite formation within, or escape from infected hepatocytes.

To evaluate the number of hepatic merozoites formed in *lisp1* mutant LS, adherent HepG2 cells, co-infected with Lisp1ΔGreen and WTRed sporozoites, were recovered after 65 h and mechanically disrupted to release the merozoites. The ratio of Lisp1ΔGreen to WTRed merozoites was ~1 (Fig. 4, left panel cells, hMZ), indicating that mutant parasites generated normal numbers of merozoites. Next, the infectivity of mutant merozoites was tested. When the approximately 1:1 ratio of Lisp1ΔGreen to WTRed merozoites collected from the disrupted HepG2 cells was injected into mice, the same ratio was found in the ensuing blood stages (Fig. 4, left panel cells, iRBC). Further, when supernatants from the mixed infections collected at 65 h were injected intravenously into mice, the ratio of Lisp1ΔGreen : WTRed blood-stage parasites (Fig. 4, right, supernatant) was the same as the ratio of injected hepatic merozoites and was maintained after several multiplication cycles, showing that the merozoites released from *lisp1* mutant LS were indeed infectious (see also Fig. S5) and had similar infectivity to red blood cells compared with WT.

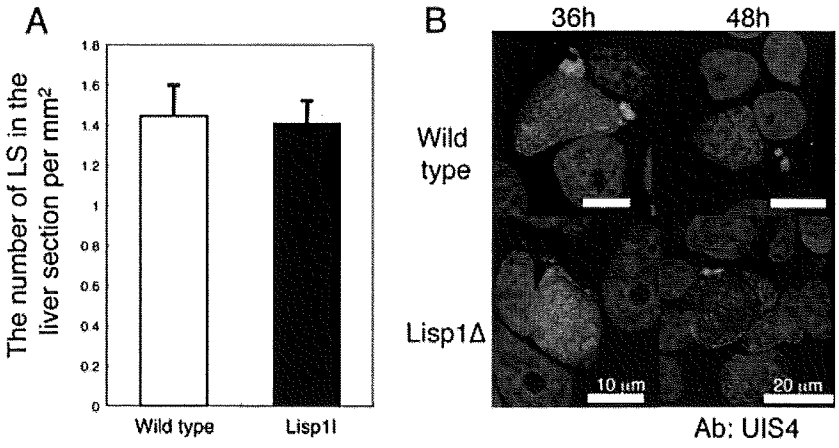

Fig. 3. *Lisp1*-defective parasites develop normally, within a PVM, into late-stage LS.
A. Histogram representation of the number of LS *in vivo*. A total of 300 000 wild-type or Lisp1l sporozoites were injected intravenously into rats and 48 h later the number of WT (white box) and Lisp1l (black box) LS were counted in the liver sections. Bars indicate the standard deviation from three rats.
B. Confocal micrograph of PVM in *Lisp1*-defective parasites. HepG2 cells 36 and 48 h post infection with WT (Wild type) or Lisp1ΔGreen sporozoites. LS parasites (green) labelled with an anti-UIS4 antibody (red) and nuclei stained with DAPI (blue).

Table 1. The ratio of merozoites released from HepG2 cells co-infected with either WTGreen and WTRed or Lisp1ΔGreen and WTRed sporozoites.

Experiment No.	WTGreen : WTRed	Lisp1ΔGreen : WTRed
1	1.1:1	0.20:1
2	1.0:1	0.10:1
3	1.1:1	0.24:1
4		0.12:1
5		0.059:1
6	0.8:1	0.12:1
7		0.11:1
Ave	1.0:1	0.11:1

The average (Ave) ratio from seven independent experiments is shown.

Taken together, these data indicate that in the absence of LISP1 infectious merozoites are formed normally but are not released efficiently from the LS.

Mutant LS do not rupture the PVM

We next examined the morphology of late stages of LS development by transmission electron microscopy (TEM). HepG2 cells were infected with WTGreen or Lisp1ΔGreen sporozoites, and 58 or 61 h later the infected cells were isolated by fluorescence-activated cell sorting and processed for TEM. As shown in Fig. 5A, there was no difference between the development of WT and *Lisp1* mutant parasites at 58 h. Indeed, the proportion of LS containing morphologically mature merozoites was very similar (20–30%). However, about 50% of the WT parasites were no longer surrounded by a visible PVM (Fig. 5B and C) whereas the majority of *Lisp1* mutant parasites were packed within a membrane (Fig. 5D). At 61 h, we were unable to observe WT LS containing merozoites presumably because the breakdown of the PVM rendered them too fragile to survive the sorting procedure. On the contrary, mutant-infected cells were found and the majority of these contained numerous merozoites inside a visible PVM (Fig. 5E and F). The ultrastructure of these merozoites appeared normal as assessed by the presence of a nucleus, rhoptries and a membrane coat (see Fig. S6). These observations strongly support the role of LISP1 in the PVM breakdown and merozoite egress from the host cell.

SERA1 localization is modified in LISP1-defective LS

Several lines of evidence strongly suggest that SERA cysteine proteases play an important role in the rupture of the PVM (Sturm *et al.*, 2009) so we assessed the distribution of SERA-1 protein in LISP1-defective LS. HepG2 cells were infected with WTGreen or Lisp1ΔGreen sporozoites and 48 h later the LS were stained with anti-SERA1 antibody. In WT LS the distribution of SERA gave a punctuated signal located at the PVM whereas in the mutant LS, the signal was more diffuse and possibly extended beyond the PVM (Fig. 6 and Fig. S7). These data show that in the absence of LISP1 the distribution of SERA1 is modified.

Discussion

Egress from the host cell is a fundamental and recurrent step of the *Plasmodium* life cycle. Evidence has now accumulated indicating that the process occurs in two distinct steps, with the rupture of the PVM preceding the rupture of the host cell membrane. The molecular bases of these processes, however, remain unknown.

Earlier work performed with erythrocytic forms of the parasite (reviewed in Blackman, 2008) has suggested that the breakdown of the PV and erythrocyte membranes both depend on proteases but have distinct bases, since treatment with E64, a cysteine protease inhibitor, selectively blocks PVM rupture. Several lines of evidence suggest that the cysteine proteases of the serine repeat antigen (SERA) family (Debrabant *et al.*, 1992), which share a central papain-like domain, play a major role in these processes. This gene family contains nine members in *P. falciparum* and five in rodent-infecting species (Arisue *et al.*, 2007). In *P. falciparum*, SERA proteins are expressed late during the schizogonic cycle (Hodder *et al.*, 2003; Le Roch *et al.*, 2003; 2004) and accumulate in the PV lumen (Knapp *et al.*, 1989; 1991), and the paralogues encoding SERA5 and SERA6 cannot be inactivated (Miller *et al.*, 2002a,b; McCoubrie *et al.*, 2007). In *P. berghei*, four of the five SERA-encoding genes are

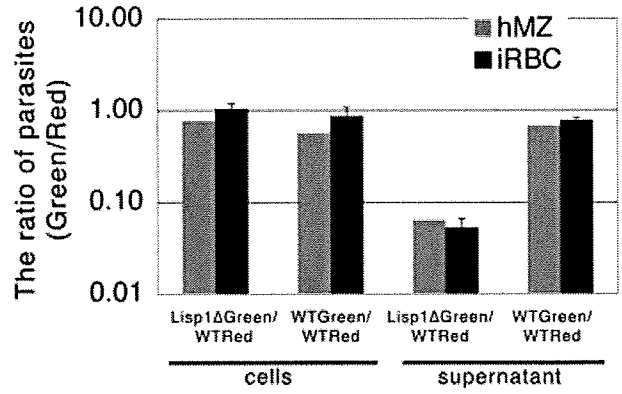

Fig. 4. *Lisp1* mutant LS parasites are defective in the release of merozoites. Graph showing the ratio of Green : Red hepatic merozoites (hMZ) collected at 65 h from adherent HepG2 cells (left) or the supernatant (right) co-infected with Lisp1ΔGreen and WTRed or WTGreen and WTRed sporozoites and the ratios found in blood stages (iRBC) after injection of these merozoites into mice. The results obtained from the supernatant and adherent cells are indicated. The average and standard deviation from four mice are shown.

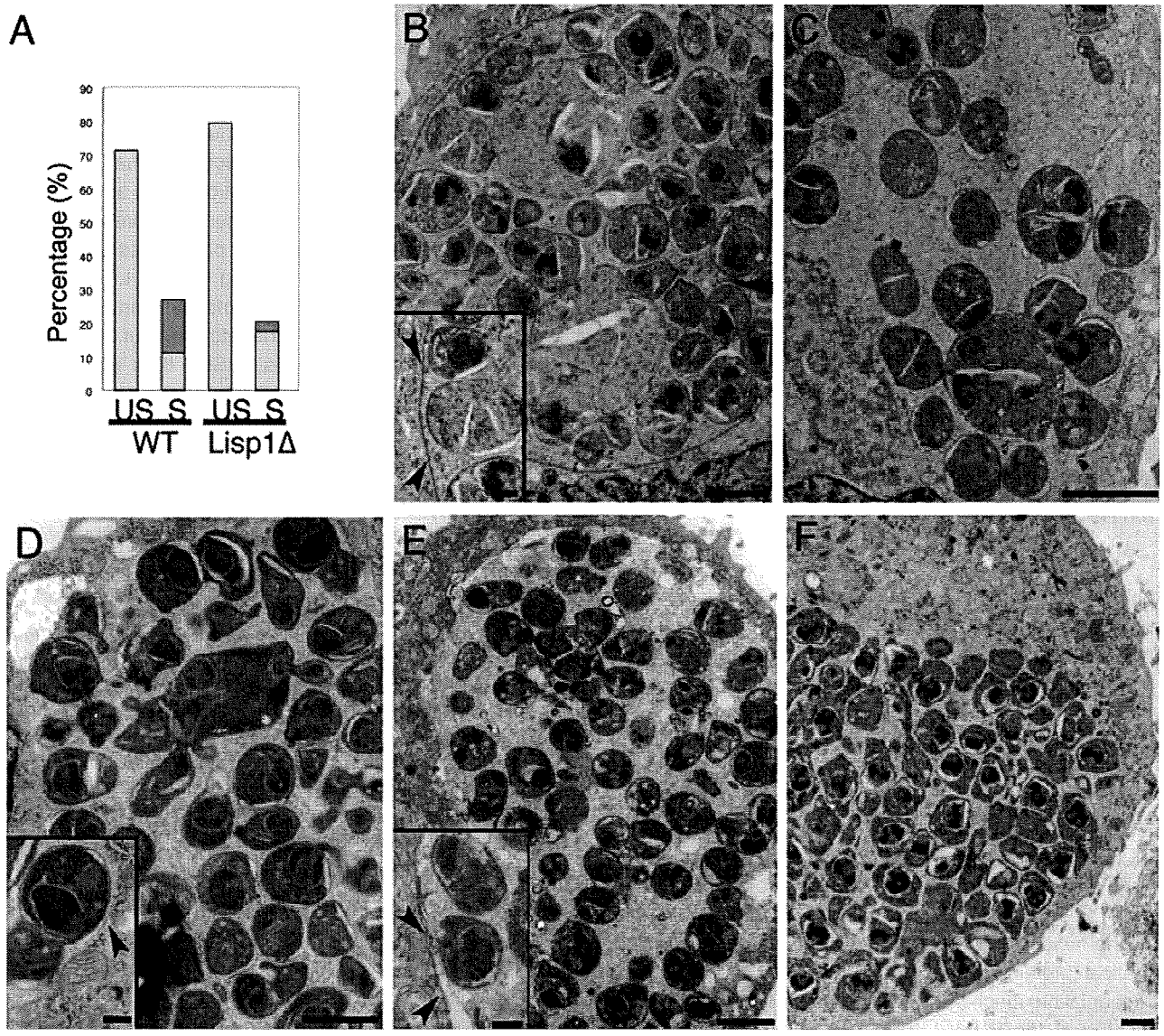

Fig. 5. *Lisp1* mutant merozoites remain within a PVM.
A. Histogram of the percentage of 58 h WTGreen and Lisp1ΔGreen unsegmented LS with no merozoites (US, lilac), and segmented LS containing merozoites (S) with (yellow) or without (orange) a visible PVM.
B–F. Representative examples of hepatic schizonts 58 h (B–D) and 61 h (E and F) post infection. (B) WTGreen with PVM; (C) WTGreen without PVM; (D) Lisp1Δ LS with PVM; (E and F) Lisp1Δ LS at 61 h containing many merozoites within a membrane boundary; scale bars are 2 μm. Insets show mature merozoites; scale bar is 500 nm and arrow heads indicate membrane.

upregulated late during LS maturation, and SERA2 and SERA3 are released in the hepatocyte cytoplasm during merozoite formation (Schmidt-Christensen *et al.*, 2008). Cysteine protease activity is known to be important for the destruction of the LS-enclosing PVM, as well as in the subsequent liberation of merosomes, since the two processes are E64-sensitive (Sturm *et al.*, 2006; Sturm and Heussler, 2007). The available data thus indicate that the SERA cysteine proteases play an important role in the disruption of the PVM, although some additional, non-cysteine protease activity is probably required for disrupting the host cell membrane. Gene targeting in *P. berghei* also showed that SERA8, called egress cysteine protease 1 (ECP1), is important for sporozoite egress from extracellular oocysts in the gut of the mosquito vector, inside which parasites extensively multiply (Aly and Matuschewski, 2005).

We have characterized here a novel protein, LISP1, which is produced by late LS and associates with their enclosing PVM. Inactivation of *Lisp1* in *P. berghei* decreased 15-fold the LS capacity to generate a blood infection in mice. *In vitro*, LISP1-deficient hepatic mero-

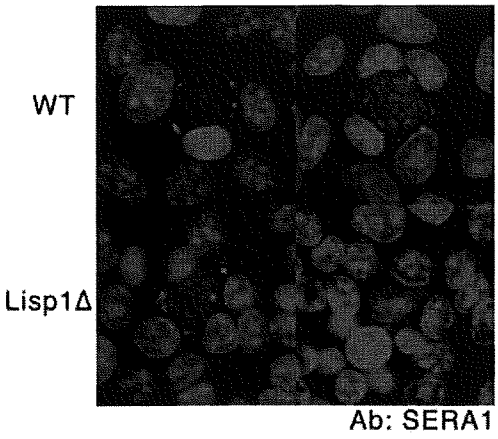

Fig. 6. Localization of SERA1 is modified in *Lisp1* mutant LS parasites. HepG2 cells were infected with wild type (WT, top) or Lisp1ΔGreen sporozoites (Lisp1Δ, bottom) and 48 h later the LS were stained an anti-SERA1 antibody (red) and nuclei stained with DAPI (blue).

zoites were normally formed inside HepG2 cells, and displayed normal infectivity to erythrocytes. This indicates that LISP1 does not play an important role in the function of the PVM, either as a structural protein or as a transporter. However, the PVM of defective LS was not degraded and the merozoites remained trapped inside hepatocytes. The timing of LISP1 production, its localization and the phenotype of the defective mutant thus suggest that LISP1 plays an important role in the rupture of the LS-enclosing PVM. Nevertheless, since LISP1-deficient parasites give rise to a delayed blood infection in mice, release of some merozoites can occur.

The molecular function of LISP1, annotated as a hypothetical protein with a predicted signal peptide but no recognizable functional domain, remains unknown. Being located at the PVM, LISP1 might act as a membrane receptor of the proteases and/or might be involved in their activation/processing at the membrane. In erythrocytic merozoites, processing of the SERA proteases depends on the subtilisin-like serine protease SUB1, which is abundant in schizont stages and is discharged from organelles named exonemes into the PV just prior to egress (Yeoh *et al.*, 2007). LISP1 might thus participate in the further processing of SERA proteases at the PVM, activating their membrane-destabilizing capacity. In the absence of LISP1, the SERA proteins might still be secreted through the PVM without being activated, hence the observed phenotype. Alternatively, LISP1 might be a target of the proteases, mediating membrane dislocation itself upon hydrolysis or processing. Finally, since LISP1 was not detected at the hepatocyte membrane, it seems unlikely that it is also directly involved in merosome formation and hepatocyte/merosome membrane disruption.

Most members of the Apicomplexa phylum, to which *Plasmodium* belongs, invade host cells and multiply within the confines of a PVM that they must eventually breach (Blackman, 2008). In spite of this conserved behaviour, it is striking that all *Plasmodium* products identified so far as being involved in the function/structure of the PVM, such as the ETRAMPs, or in its disruption, such as the SERA proteases, are specific to the genus. Moreover, these products come in stage-specific paralogues adapted to the particular host cell harbouring the PV. LISP1, which appears to be specific to the *Plasmodium* genus, is important for parasite egress from hepatocytes but dispensable for egress from erythrocytes. LISP1 thus adds to the notion of exquisitely specific mechanisms involved in the lysis of the PVM by Apicomplexa parasites.

Experimental procedures

P. berghei *strains and the infection of mice, rats and mosquitoes*

ANKAGreen is ANKA 507m6cL1 which expresses GFP from the *eef1α* promoter (Janse *et al.*, 2006a) and was obtained from MR4 (MRA-867), deposited by C.J. Janse and A.P. Waters; ANKARed (ANKA L733), expressing RFP from *eef1α* promoter, is described in Sturm *et al.* (2009). Infection of mice, *Anopheles stephensi* mosquitoes and isolation of salivary gland sporozoites were performed as previously described (Thiberge *et al.*, 2007). All studies on animals followed the guidelines on the ethical use of animals from the European Communities Council Directive of 24 November 1986 (86/609/EEC).

Real-time reverse transcription polymerase chain reaction (RT-PCR)

Two independent total RNA preparations were made from mixed infected blood stages, salivary gland sporozoites at day 21 post infection and HepG2 cells 5, 17, 40 and 50 h post infection. PCR conditions were one cycle at 95°C for 10 min, 40 cycles at 95°C for 15 s, 55°C for 15 s and 60°C for 45 s. *Lisp1* gene expression was normalized by the *hsp70* (PB001074.01.0) gene expression in each sample. Analysis was performed using the ΔCt method (User Bulletin 2, Applied Biosystems) using the blood stages as reference.

Primers used: *lisp1*F 5′-GCCAAATGCTAAACCTAATG-3′; *lisp1*R 5′-TGGGTTTGTATTGTATGCAC-3′; *hsp70*F 5′-TGCAGC AGATAATCAAACTC-3′; *hsp70*R: 5′-ACTTCAATTTGTGGAACA CC-3′.

Rabbit anti-LISP1 antibody preparation

LISP1 amino acids 1392–1437 were fused to glutathione S-transferase (GST) using the pGEX 6P-1 system (Amersham Bioscience, Uppsala, Sweden). The protein was purified on a GST column and used to immunize rabbits. Specific antibodies were affinity purified on an *N*-hydroxysuccinimide-activated column (Amersham Bioscience) coupled with recombinant protein. The antibody titre was 1.07 mg ml^{-1}.

Immunofluorescence analysis

Purified parasites were fixed in acetone for 2 min and the samples incubated with rabbit anti-LISP1 antibodies then FITC-conjugated secondary antibody (Zymed, South San Francisco, CA, USA). For nuclear staining, 0.02 μg ml^{-1} 4′, 6-diamidino-2-phenylindole (DAPI) was added to the secondary antibody solution.

For IFA of LS in infected HepG2 cells, fixation was either 4% paraformaldehyde (PFA) + 0.1% triton or acetone, and incubation was with anti-LISP1 antibodies and Alexa 647-conjugated secondary antibody. PFA (4%) fixation and 0.1% triton permeabilization were used with the anti-UIS4 antibody. Methanol fixation was used with anti-EXP1 and anti-SERA1 antibodies.

Targeted disruption of lisp1 *and genotypic analysis*

Construction of the lisp1l *targeting vector.* Two fragments of 853 and 801 bp were amplified from genomic DNA with primers: 5′-GGGGAGCTCGTCTATTTTTGATACGATATGTGCACATGC-3′ and 5′-GGGGGATCCCTTGAAGGCGATTAACTATATTGTCGC-3′; 5′-GGGCTCGAGCGAATCAGTGTCGCTTGATATTTTG-3′ and 5′-GGGGGTACCCTGGGTTTGTATTGTATGCACCTAAGG-3′ and cloned either side of the selectable marker gene in pBluescript (Stratagene, La Jolla, CA, USA). For Southern analysis ANKA genomic DNA was digested with SphI and hybridized with a probe made from amplification with primers: 5′-GGG GAGCTCGTCTATTTTTGATACGATATGTGCACATGC-3′ and 5′-GGGGGATCCCTTGAAGGCGATTAACTATATTGTCGC-3′.

Construction of the Lisp1Δ *targeting vector.* Two fragments of 630 and 600 bp were amplified from genomic DNA with primers 5′-CGATGCGGGCCCGAGAATACAACTTACTAGGAAATGCAC-3′ and 5′-AGCTGGCGCGCCCTTGCATCTTCAGACATGTTA TTTTCGA-3′; 5′-CCAGTGAGTGCGGCCGCGGCTAAAGCTCG ATGTCGTATTCAAGAA-3′ and 5′-AGCTGGCGCGCCCTGGG AATTTTTCAATTTCTTCCATTTG-3′. These primers were tailed with restriction sites for ApaI, SmaI, NotI and AscI respectively. The fragments were cloned in the vector pBC-hDHFR vector (B. Boisson, unpublished). This vector is pBC SK (+) (Stratagene), modified to introduce an AscI restriction site, and contains a human dihydrofolate reductase (hDHFR) selection cassette with the 5′ untranslated region of the *eef1α* gene and the 3′ untranslated region of the DHFR-TS gene cloned between SmaI and NotI of pBC SK (+). Transfection and selection of recombinant parasites was performed as previously described (Janse *et al.*, 2006b). Southern analysis was performed on SphI-restricted genomic DNA hybridized with the probe indicated on Fig. S2.

Evaluation of sporozoite infectivity in vivo

Sporozoites collected from mosquito salivary glands were injected intravenously into 3-week-old female Wistar rats (Japan SLC, Hamamatsu, Japan) ($n = 5$) or 4-week-old C57BL/6 mice (Janvier, France). Parasitaemias were checked at indicated time points by Geimsa-stained blood smear.

LS development assay in vivo

A total of 300 000 Lisp1l or WT sporozoites were injected into 3-week-old Wistar rats and 48 h later, the livers were perfused with phosphate-buffered saline (PBS) then 4% PFA. After inclusion in 20% sucrose, 20 μm frozen sections were prepared on a Leica cryostat. The sections were stained with anti-CS antiserum and the number of LS in six sections from each rat was counted. A total of 1619 Lisp1l, 1877 WT LS were counted.

LS development in HepG2 cells

HepG2 cells were grown in DMEM + Glutamax-1 media (Gibco) supplemented with 10% FCS (PAA laboratories GmbH) at 37°C in the presence of 5% CO_2. The day before infection $4–5.0 \times 10^4$ were plated per well in eight-well chamber slides (Nalge Nunc International, Rochester, NY, USA) and 24 h later WT and/or mutant sporozoites (5.0×10^4) were added. The medium was changed daily. The LS were detected by immunofluorescence staining as described above.

Real-time imaging of LS development in HepG2 cells

HepG2 cells were co-infected with WTRed and Lisp1ΔGreen sporozoites. The development of 27 WT and 28 mutant LS was followed from 24 to 48 h post infection by acquisition of images at 60 min intervals with a PerkinElmer spinning disc confocal microscope. The area was calculated using ImageJ software.

Detection of LISP1 by immunoblot

HepG2 cells were infected with WTGreen or Lisp1ΔGreen sporozoites as described above. After 48 h the cells from each well were lysed in Novex® Tris-Glycine sodium dodecyl sulfate (SDS) sample buffer (Invitrogen) and immediately stored at −80°C. Prior to loading on a 4–15% gradient acrylamide gel (Bio-Rad), β mercaptoethanol was added (0.7 M final) and the samples were heated for 5 min at 95°C. Molecular weight markers were Precision Plus Protein (Bio-Rad). After electrophoresis the proteins were transferred to a Hybond-ECL nitrocellulose membrane (Amersham Biosciences). The membrane was first incubated with a 1:2000 dilution of the anti-LISP1 antibody then with a 1:10 000 dilution of a chicken anti-rabbit IgG horseradish peroxidase (HRP)-conjugated antibody (Santa Cruz). The presence of antibodies was revealed with the SuperSignal® West Femto kit (Thermo Scientific). The membrane was then incubated with a 1:10 000 dilution of HRP-conjugated rabbit polyclonal anti-GAPDH (glyceraldehyde-3-phosphate dehydrogenase) (Santa Cruz) and the same kit used to reveal the presence of antibodies. The signals were scanned using Quantity One software (Bio-Rad) and quantified with NanoDrop ND-1000 software (Thermo Fischer Scientifique).

Estimation of number of hepatic merozoites

HepG2 cells were co-infected with equal numbers of either WTRed and WTGreen or WTRed and Lisp1ΔGreen sporozoites. Sixty-five hours later the supernatants were taken, centrifuged for 3 min at 12 000 r.p.m. and the pellet re-suspended in PBS. Cells were scraped from the wells and mechanically disrupted by passing through a Omnican® 30G insulin needle. The samples were placed on Ibidi slides and observed with a Zeiss Axio observer Z1 microscope.

TEM analysis of infected HepG2 cells

WTGreen or Lisp1ΔGreen sporozoites were added to HepG2 cells and 58 or 61 h later cells were collected, fixed with 0.4% PFA and GFP-positive cells enriched by sorting on a FACSAria (BD Biosciences). Sorted cells were fixed with 2.5% glutaraldehyde in 0.1 M cacodylate buffer at 4°C for 24 h. Then, cell pellets were embedded in agarose type IV (Sigma, Chemical, Saint Louis, USA). After several washes in 0.1 M cacodylate buffer, samples were post-fixed for 1 h with 1% osmium tetroxide (Merck, Darmstadt, Germany) in the same buffer. After dehydration in a graded ethanol series, the samples were embedded in Epon resin and polymerized. Contrasted ultra-thin sections (60 nm) were observed in a JEM 1010 Transmission Elecron Microscope (Jeol, Tokyo, Japan). A total of 103 Lisp1ΔGreen and 62 WT LS were observed at 58 h.

Statistical analysis

The data presented in Figs 1A, 2E and 3A were analysed by a Kruskal–Wallis rank sum test. The data presented in Fig. 4 were analysed by a Mann–Whitney test.

Data deposition

Sequences from the EST libraries were deposited in the DDBJ website 2007. The LISP1 sequence reported in this article has been deposited in the GenBank database (Accession No. AB231328).

Acknowledgements

T.I. was supported by the Japan Society for the Promotion of Science (JSPS) as JSPS Postdoctoral Fellowships for Research Abroad. B.B. was supported by the Fonds dédiés 'Combattre les maladies Parasitaires' financed by the Ministère de la Recherche and Sanofi-Aventis. We are extremely grateful to Dr Kappe for providing the anti-UIS4 antibody, Drs Thomas and Barale for the anti-AMA1 antibody, Dr Heussler for anti-EXP1 and anti-SERA1 antibodies. We thank Ms Naoko Kimura for maintenance of mosquitoes and Ms Izumi Kaneko and Ms Tomomi Kato for technical assistance. C. Bourgouin, I. Thiery and the other members of the 'Centre de Production et d'Infection des Anophèles' (Institut Pasteur) are thanked for mosquito rearing. We thank Dr Marie Nguyen-De Bernon Plate-forme de Cytometrie for cell sorting. We also thank Dr Rogerio Amino for help with real-time imaging and all members of BGP for stimulating discussions and comments. This work was supported by funds from the Institut Pasteur, the Howard Hughes Medical Institute and the European Commission (FP6 BioMalPar Network of Excellence). R.M. is a Howard Hughes Medical Institute International Scholar.

References

Aikawa, M. (1971) Parasitological review. *Plasmodium*: the fine structure of malarial parasites. *Exp Parasitol* **30:** 284–320.

Aly, A.S., and Matuschewski, K. (2005) A malarial cysteine protease is necessary for *Plasmodium* sporozoite egress from oocysts. *J Exp Med* **202:** 225–230.

Arisue, N., Hirai, M., Arai, M., Matsuoka, H., and Horii, T. (2007) Phylogeny and evolution of the SERA multigene family in the genus *Plasmodium*. *J Mol Evol* **65:** 82–91.

Baer, K., Klotz, C., Kappe, S.H., Schnieder, T., and Frevert, U. (2007) Release of hepatic *Plasmodium yoelii* merozoites into the pulmonary microvasculature. *PLoS Pathog* **3:** e171.

Bano, N., Romano, J.D., Jayabalasingham, B., and Coppens, I. (2007) Cellular interactions of *Plasmodium* liver stage with its host mammalian cell. *Int J Parasitol* **37:** 1329–1341.

Blackman, M.J. (2008) Malarial proteases and host cell egress: an 'emerging' cascade. *Cell Microbiol* **10:** 1925–1934.

Charpian, S., and Przyborski, J.M. (2008) Protein transport across the parasitophorous vacuole of *Plasmodium falciparum*: into the great wide open. *Traffic* **9:** 157–165.

Debrabant, A., Maes, P., Delplace, P., Dubremetz, J.F., Tartar, A., and Camus, D. (1992) Intramolecular mapping of *Plasmodium falciparum* P126 proteolytic fragments by N-terminal amino acid sequencing. *Mol Biochem Parasitol* **53:** 89–95.

Doolan, D.L., Hedstrom, R.C., Rogers, W.O., Charoenvit, Y., Rogers, M., de la Vega, P., *et al.* (1996) Identification and characterization of the protective hepatocyte erythrocyte protein 17 kDa gene of *Plasmodium yoelii*, homolog of *Plasmodium falciparum* exported protein 1. *J Biol Chem* **271:** 17861–17868.

Hodder, A.N., Drew, D.R., Epa, V.C., Delorenzi, M., Bourgon, R., Miller, S.K., *et al.* (2003) Enzymic, phylogenetic, and structural characterization of the unusual papain-like protease domain of *Plasmodium falciparum* SERA5. *J Biol Chem* **278:** 48169–48177.

Janse, C.J., Franke-Fayard, B., and Waters, A.P. (2006a) Selection by flow-sorting of genetically transformed, GFP-expressing blood stages of the rodent malaria parasite, *Plasmodium berghei*. *Nat Protoc* **1:** 614–623.

Janse, C.J., Franke-Fayard, B., Mair, G.R., Ramesar, J., Thiel, C., Engelmann, S., *et al.* (2006b) High efficiency transfection of *Plasmodium berghei* facilitates novel selection procedures. *Mol Biochem Parasitol* **145:** 60–70.

Knapp, B., Hundt, E., Nau, U., and Kupper, H.A. (1989) Molecular cloning, genomic structure and localization in a blood stage antigen of *Plasmodium falciparum* characterized by a serine stretch. *Mol Biochem Parasitol* **32:** 73–83.

Knapp, B., Nau, U., Hundt, E., and Kupper, H.A. (1991) A new blood stage antigen of *Plasmodium falciparum* highly homologous to the serine-stretch protein SERP. *Mol Biochem Parasitol* **44:** 1–13.

Le Roch, K.G., Zhou, Y., Blair, P.L., Grainger, M., Moch, J.K., Haynes, J.D., *et al.* (2003) Discovery of gene function by expression profiling of the malaria parasite life cycle. *Science* **301:** 1503–1508.

Le Roch, K.G., Johnson, J.R., Florens, L., Zhou, Y., Santrosyan, A., Grainger, M., *et al.* (2004) Global analysis of transcript and protein levels across the *Plasmodium falciparum* life cycle. *Genome Res* **14:** 2308–2318.

Lingelbach, K., and Joiner, K.A. (1998) The parasitophorous vacuole membrane surrounding *Plasmodium* and *Toxo-*

plasma: an unusual compartment in infected cells. *J Cell Sci* **111:** 1467–1475.
McCoubrie, J.E., Miller, S.K., Sargeant, T., Good, R.T., Hodder, A.N., Speed, T.P., *et al.* (2007) Evidence for a common role for the serine-type *Plasmodium falciparum* serine repeat antigen proteases: implications for vaccine and drug design. *Infect Immun* **75:** 5565–5574.
Matuschewski, K., Ross, J., Brown, S.M., Kaiser, K., Nussenzweig, V., and Kappe, S.H. (2002) Infectivity-associated changes in the transcriptional repertoire of the malaria parasite sporozoite stage. *J Biol Chem* **277:** 41948–41953.
Meis, J.F., and Verhave, J.P. (1988) Exoerythrocytic development of malarial parasites. *Adv Parasitol* **27:** 1–61.
Miller, L.H., Baruch, D.I., Marsh, K., and Doumbo, O.K. (2002a) The pathogenic basis of malaria. *Nature* **415:** 673–679.
Miller, S.K., Good, R.T., Drew, D.R., Delorenzi, M., Sanders, P.R., Hodder, A.N., *et al.* (2002b) A subset of *Plasmodium falciparum* SERA genes are expressed and appear to play an important role in the erythrocytic cycle. *J Biol Chem* **277:** 47524–47532.
Mueller, A.K., Labaied, M., Kappe, S.H., and Matuschewski, K. (2005a) Genetically modified *Plasmodium* parasites as a protective experimental malaria vaccine. *Nature* **433:** 164–167.
Mueller, A.K., Camargo, N., Kaiser, K., Andorfer, C., Frevert, U., Matuschewski, K., *et al.* (2005b) *Plasmodium* liver stage developmental arrest by depletion of a protein at the parasite–host interface. *Proc Natl Acad Sci USA* **102:** 3022–3027.
Schmidt-Christensen, A., Sturm, A., Horstmann, S., and Heussler, V.T. (2008) Expression and processing of *Plasmodium berghei* SERA3 during liver stages. *Cell Microbiol* **10:** 1723–1734.
Simmons, D., Woollett, G., Bergin-Cartwright, M., Kay, D., and Scaife, J. (1987) A malaria protein exported into a new compartment within the host erythrocyte. *EMBO J* **6:** 485–491.
Spielmann, T., Gardiner, D.L., Beck, H.P., Trenholme, K.R., and Kemp, D.J. (2006) Organization of ETRAMPs and EXP-1 at the parasite–host cell interface of malaria parasites. *Mol Microbiol* **59:** 779–794.
Sturm, A., and Heussler, V. (2007) Live and let die: manipulation of host hepatocytes by exoerythrocytic *Plasmodium* parasites. *Med Microbiol Immunol* **196:** 127–133.
Sturm, A., Amino, R., van de Sand, C., Regen, T., Retzlaff, S., Rennenberg, A., *et al.* (2006) Manipulation of host hepatocytes by the malaria parasite for delivery into liver sinusoids. *Science* **313:** 1287–1290.
Sturm, A., Graewe, S., Franke-Fayard, B., Retzlaff, S., Bolte, S., Roppenser, B., *et al.* (2009) Alteration of the parasite plasma membrane and the parasitophorous vacuole membrane during exo-erythrocytic development of malaria parasites. *Protist* **160:** 51–63.
Tarun, A.S., Dumpit, R.F., Camargo, N., Labaied, M., Liu, P., Takagi, A., *et al.* (2007) Protracted sterile protection with *Plasmodium yoelii* pre-erythrocytic genetically attenuated parasite malaria vaccines is independent of significant liver-stage persistence and is mediated by CD8+ T cells. *J Infect Dis* **196:** 608–616.
Tarun, A.S., Peng, X., Dumpit, R.F., Ogata, Y., Silva-Rivera, H., Camargo, N., *et al.* (2008) A combined transcriptome and proteome survey of malaria parasite liver stages. *Proc Natl Acad Sci USA* **105:** 305–310.
Thiberge, S., Blazquez, S., Baldacci, P., Renaud, O., Shorte, S., Ménard, R., *et al.* (2007) *In vivo* imaging of malaria parasites in the murine liver. *Nat Protoc* **2:** 1811–1818.
Wickham, M.E., Culvenor, J.G., and Cowman, A.F. (2003) Selective inhibition of a two-step egress of malaria parasites from the host erythrocyte. *J Biol Chem* **278:** 37658–37663.
Yeoh, S., O'Donnell, R.A., Koussis, K., Dluzewski, A.R., Ansell, K.H., Osborne, S.A., *et al.* (2007) Subcellular discharge of a serine protease mediates release of invasive malaria parasites from host erythrocytes. *Cell* **131:** 1072–1083.

Supporting information

Additional Supporting Information may be found in the online version of this article:

Fig. S1. Histogram representation of real-time RT-PCR analysis of *lisp1* relative gene expression in rat livers 24, 48 and 60 h post infection. Total liver RNA was isolated 24, 48 and 60 h post infection with RNAgents Total RNA Isolation System (Promega, Madison, WI, USA) and cDNAs made. Lisp1 was amplified with primers 5′-GCCCCCTGGCGATCTTAATTT-3′ and 5′-TAAACG TTTCAGGGGGCGAT-3′. The expression was normalized to rat glyceraldehyde-3-phosphate dehydrogenase, amplified with primers 5′-TGATTCTACCCACGGCAAGTT-3′ and 5′-TGATGGG TTTCCCATTGATGA-3′. Error bars are standard deviation.
Fig. S2. Gene inactivation of *lisp1*.
A. Double-crossing-over strategy used to generate Lisp1l mutant parasites. Genomic DNA of ANKA (WT) and two clones of Lisp1l digested with SphI and hybridized with a 5′ probe indicated by a thick black line.
B. Double-crossing-over strategy used to generate Lisp1Δ clones in NK65 and WTGreen. Genomic DNA was digested with SphI and hybridized with a 5′ probe indicated by a thick black line.
Fig. S3. Infectivity of Lisp1ΔGreen sporozoites compared with WTGreen (wild type). A total of 25 000 salivary gland sporozoites were injected intravenously into C57Bl/6 mice and blood-stage parasitaemias checked daily. Bars indicate standard errors.
Fig. S4. The size of *lisp1*-defective LS is normal.
A. Histogram representation of the size of LS in HepG2 cells co-infected with WTRed (Wild type, white box) and Lisp1ΔGreen (black box) sporozoites. The LS parasites were detected by their fluorescence and imaged by spinning disk confocal microscopy and the relative area calculated with ImageJ software.
B. Sample of sorted HepG2 cells 58 h post infection with WTGreen (top) or Lisp1ΔGreen sporozoites used for TEM.
Fig. S5. Lisp1l merozoites express AMA1. Merozoites collected from the supernatant of HepG2 cells infected with ANKA and Lisp1l sporozoites were incubated with an anti-AMA1 antibody and Alexa 546-conjugated secondary antibody.
Fig. S6. Transmission electron micrographs of WT and mutant LS 59 h post infection.
A. WT LS with numerous merozoites in the host cytoplasm and absence of PVM. The aspect of the nucleus indicates that the cell is dying.
B. Lisp1ΔGreen LS with many merozoites and a visible PVM.

C and D. Detail of Lisp1ΔGreen hepatic merozoites. The merozoites appear normal at the ultrastructural level with the presence of a nucleus, rhoptry and coated membrane.

Fig. S7. Immunofluorescence analysis of LS 48 h post infection of HepG2 cells with WT sporozoites. Samples were incubated with an anti-LISP1 antibody and an anti-SERA1 antibody followed by Alexa-conjugated secondary antibodies. LISP1 labelling in green, left; SERA1 labelling in red, centre; merged image, right.

Please note: Wiley-Blackwell are not responsible for the content or functionality of any supporting materials supplied by the authors. Any queries (other than missing material) should be directed to the corresponding author for the article.

Brief report

Gene expression profiling of peripheral T-cell lymphoma including γδ T-cell lymphoma

Kana Miyazaki,[1] Motoko Yamaguchi,[1] Hiroshi Imai,[2] Tohru Kobayashi,[1] Satoshi Tamaru,[1] Kazuhiro Nishii,[1] Masao Yuda,[3] Hiroshi Shiku,[4] and Naoyuki Katayama[1]

Departments of [1]Hematology and Oncology, [2]Pathologic Oncology, [3]Medical Zoology, and [4]Cancer Vaccine and Immuno-Gene Therapy, Mie University Graduate School of Medicine, Tsu, Japan

The gene expression profile of peripheral γδ T-cell lymphoma (γδTCL) has not been investigated. Using oligonucleotide microarrays, we analyzed total RNA from 7 patients with γδTCL (4 hepatosplenic, 1 cutaneous, 1 intestinal, and 1 thyroidal) and 27 patients with αβTCL (11 peripheral TCL-unspecified, 15 angioimmunoblastic TCL, and 1 hepatosplenic). Unsupervised microarray analyses classified all hepatosplenic γδTCLs into a single cluster, whereas other γδTCLs were scattered within the αβTCL distribution. We identified a T-cell receptor signature gene set, which accurately classified γδTCL and αβTCL. A classifier based on gene expression under supervised analysis correctly identified γδTCL. One case of hepatosplenic αβTCL was placed in the γδTCL grouping. γδTCL signature genes included genes encoding killer cell immunoglobulin-like receptors and killer cell lectin-like receptors. Our results indicate that hepatosplenic γδTCL is a distinct form of peripheral TCL and suggest that nonhepatosplenic γδTCLs are heterogeneous in gene expression. (Blood. 2009;113:1071-1074)

Introduction

T cells expressing the γδ T-cell receptor (TCR) heterodimer comprise only a small fraction of the peripheral blood T-cell population and differ from those expressing the αβ TCR in terms of development, tissue distribution, and function.[1,2] Mature T-cell lymphomas (TCLs) with the γδ T-cell immunophenotype can be divided into hepatosplenic γδTCL[3] and nonhepatosplenic γδTCL.[4] The third World Health Organization (WHO) classification system describes hepatosplenic γδTCLs and hepatosplenic αβTCLs as a single disease entity (hepatosplenic TCL) as they exhibit nearly identical clinicopathologic and cytogenetic features.[4-6]

In contrast, nonhepatosplenic γδTCL occurs in only a limited number of anatomic sites, including cutaneous, nasopharyngeal, gastrointestinal, pulmonary, and thyroidal regions.[7-10] This disease has also been called mucocutaneous γδTCL because the majority of patients show some involvement of mucocutaneous sites. Among nonhepatosplenic γδTCLs, the cutaneous form is most common and overlaps with subcutaneous panniculitis-like TCL.[11,12] Whereas primary cutaneous γδTCL is categorized as a single disease entity in the new WHO scheme,[13] other nonhepatosplenic γδTCLs remains an enigma.

γδTCLs are rare lymphoid malignancies and are difficult to diagnose, resulting from the lack of available monoclonal antibodies against γδTCR for use with paraffin-embedded tissue. Several studies have elucidated the gene expression profile of peripheral TCLs (PTCLs)[14-17] but did not evaluate γδTCL. In our current study, we performed gene expression profiling in 34 PTCLs, including 7 cases of γδTCL.

Methods

Patients/samples

Our present study assessed 34 cases of PTCL, including 11 PTCL-unspecified with αβ T-cell immunophenotype, 15 angioimmunoblastic TCLs, 1 hepatosplenic αβTCL, 4 hepatosplenic γδTCLs, 1 cutaneous γδTCL, 1 intestinal γδTCL, and 1 thyroidal γδTCL. All specimens were collected between 1987 and 2002 at Mie University Hospital and diagnosed according to the third WHO classification.[6] Tumor cell expression of cell-surface antigens and TCR heterodimer (αβ or γδ) was confirmed by immunohistochemistry using frozen sections as described previously.[9] DNA microarray studies using specimens from patients with hematopoietic malignancies were approved by the Institutional Review Committee of Mie University Graduate School of Medicine. Informed consent was obtained from these patients in accordance with the Declaration of Helsinki. The clinicopathologic features of 6 of 7 cases of γδTCL have been reported previously.[8,9] The single patient we examined with thyroidal γδTCL remains alive with no evidence of disease 13 years after diagnosis. Clinical data for all cases examined are presented in Table S1 (available on the *Blood* website; see the Supplemental Materials link at the top of the online article).

Gene expression profiling and analysis

Gene expression profiles were generated and analyzed as previously reported.[18] We used the Agilent 44K human oligonucleotide microarray (Agilent 4112F; Agilent Technologies, Palo Alto, CA), and raw gene expression data are available at the Gene Expression Omnibus (accession number GSE11946).[19] For gene expression profiling supervised by TCR heterodimer phenotype, we selected genes with an average differential expression level of more than 3.0-fold and used a one-sample *t* test with a

Submitted July 10, 2008; accepted October 11, 2008. Prepublished online as *Blood* First Edition paper, October 27, 2008; DOI 10.1182/blood-2008-07-166363.

The online version of this article contains a data supplement.

Presented in part at the Tenth International Conference on Malignant Lymphoma, Lugano, Switzerland, June 4, 2008.

The publication costs of this article were defrayed in part by page charge payment. Therefore, and solely to indicate this fact, this article is hereby marked "advertisement" in accordance with 18 USC section 1734.

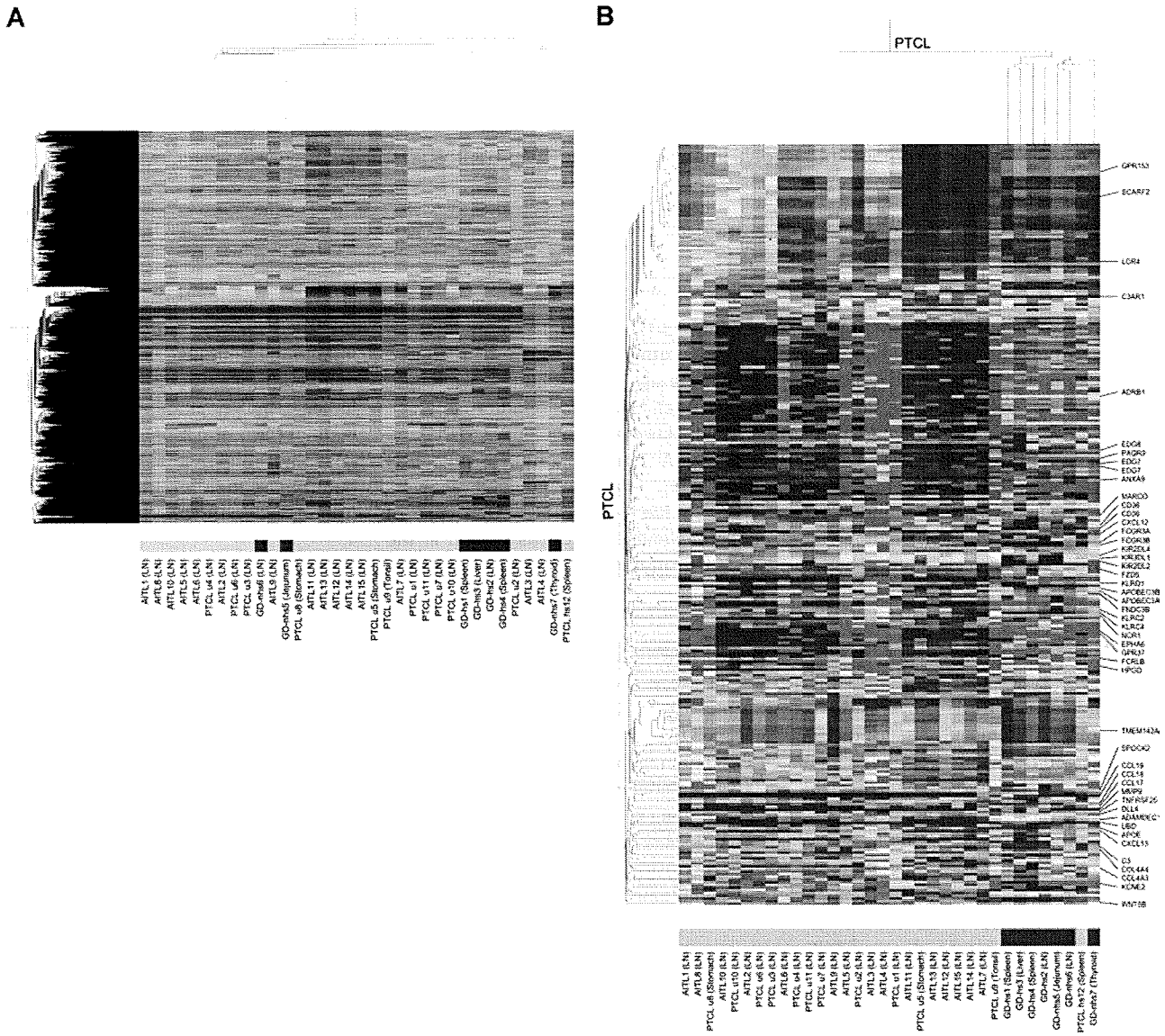

Figure 1. Hierarchical clustering of gene expression data. (A) Hierarchical clustering of 34 cases of PTCL using unsupervised analysis. Color blocks indicate the characteristics of the PTCLs; red blocks, γδTCL cases; amber blocks, αβTCL cases. The anatomic site of each specimen is shown in parentheses. AITL indicates angioimmunoblastic TCL; GD-hs, hepatosplenic γδTCL; GD-nhs, nonhepatosplenic γδTCL; LN, lymph node; PTCL hs, hepatosplenic αβTCL; PTCL u, PTCL-unspecified. Four cases of hepatosplenic γδTCL (GD-hs1-4) were classified into a single cluster. Nonhepatosplenic γδTCLs (GD-nhs5, intestinal; GD-nhs6, cutaneous; GD-nhs7, thyroidal) were scattered within the αβTCL distribution. (B) Hierarchical clustering of 34 cases of PTCL-based TCR signature gene expression. Genes also listed in Table 1 are shown on the right. γδTCL cases were correctly identified by the gene set, although one case of hepatosplenic αβTCL (PTCL hs12) was grouped with the γδTCLs.

P value cutoff of .005. Hierarchical clustering of genes was performed using the Pearson correlation, and hierarchical clustering of cases was obtained using an average linkage algorithm.

We chose WebGestalt using Gene Ontology (GO) hierarchies[20,21] for categorization of functional gene groups and the Kyoto Encyclopedia of Genes and Genomes (KEGG)[22,23] pathway for identification of signaling pathways. In both analyses, we performed a separate hypergeometric test with a *P* value cutoff of .001.

Results and discussion

Gene expression profiling is a powerful tool for establishing a molecular basis for lymphoma subtypes.[24] Unsupervised analysis of our PTCL cases classified hepatosplenic γδTCL as a single cluster, whereas other γδTCLs were scattered within the αβTCL distribution (Figure 1A). Since the 1980s, cumulative clinicopathologic evidence has demonstrated that hepatosplenic γδTCL is a distinct clinicopathologic disease entity. Our gene expression results also confirm that hepatosplenic γδTCL is distinct from other PTCLs. Conversely, nonhepatosplenic γδTCLs appeared to be more heterogeneous. The possibility that tissue differences were responsible for these data was excluded by our observation that hepatosplenic γδTCL was classified as a single cluster, irrespective of the specimen examined (Figure 1). Angioimmunoblastic TCL cases were not classified as a single cluster, consistent with prior gene expression studies.[14-17]

We next compared the gene expression profiles of γδTCL and αβTCL using 291 genes showing a greater than 3.0-fold average expression difference, which we designated the TCR signature gene set (Table S2). Of note, a classifier from supervised analysis based on gene expression identified γδTCL and hepatosplenic αβTCL (Figure 1B). This finding is supported by the notion that γδ

Table 1. GO category analysis and KEGG pathway analysis in the TCR signature gene set

Analytical tool	Gene no.	Gene	*P*
GO category			
γδTCL			
Cellular defense response	5	*KIR2DL4, NCR1, C3AR1, KLRC2, KLRC4*	1.17×10^{-4}
Signal transduction activity	29	*KLRD1, ANXA9, FNDC3B, GPR37, KIR2DL4, MARCO, EDG7, NCR1, MS4A5, HPGD, FCGR3A, LGR4, FCRLB, C3AR1, CXCL12, RTN4R, PAQR9, KLRC2, GPR153, FCGR3B, KIR2DL2, EDG8, ADRB1, CD36, FZD5, SCARF2, KIR3DL1, EPHA6, KLRC4*	5.09×10^{-6}
Receptor activity	28	*GPR37, KIR2DL4, ANXA9, KLRD1, FNDC3B, EDG7, HPGD, MARCO, LGR4, MS4A5, FCGR3A, NCR1, C3AR1, FCRLB, KLRC2, PAQR9, RTN4R, GPR153, EDG8, FCGR3B, KIR2DL2, ADRB1, FZD5, CD36, SCARF2, KIR3DL1, EPHA6, KLRC4*	7.10×10^{-8}
Transmembrane receptor activity	16	*ANXA9, GPR37, KIR2DL4, KLRD1, LGR4, HPGD, MARCO, EDG7, C3AR1, KLRC2, EDG8, GPR153, ADRB1, FZD5, EPHA6, KIR3DL1*	4.46×10^{-4}
IgG binding	2	*FCGR3A, FCGR3B*	3.07×10^{-4}
αβTCL			
Organismal physiologic process	14	*UBD, CXCL13, COL4A4, CCL18, KCNE2, CCL17, C3, TMEM142A, DLL4, APOE, COL4A3, TNFRSF25, MMP9, CCL19*	3.24×10^{-4}
Regulation of organismal physiologic process	4	*COL4A4, KCNE2, C3, APOE*	5.87×10^{-4}
Circulation	4	*KCNE2, DLL4, COL4A3, APOE*	3.14×10^{-4}
Regulation of neurophysiologic process	2	*COL4A4, APOE*	7.55×10^{-4}
Regulation of transmission of nerve impulse	2	*COL4A4, APOE*	7.55×10^{-4}
Regulation of synapse structure and function	2	*COL4A4, APOE*	8.69×10^{-4}
Regulation of synaptic transmission	2	*COL4A4, APOE*	7.55×10^{-4}
Inflammatory response	5	*CXCL13, CCL18, CCL17, C3, CCL19*	6.05×10^{-4}
Behavior	5	*CCL18, CXCL13, CCL17, APOE, CCL19*	2.47×10^{-4}
Locomotory behavior	4	*CXCL13, CCL18, CCL17, CCL19*	4.92×10^{-4}
Taxis	4	*CXCL13, CCL18, CCL17, CCL19*	4.22×10^{-4}
Chemotaxis	4	*CXCL13, CCL18, CCL17, CCL19*	4.22×10^{-4}
Receptor binding	9	*ADAMDEC1, CCL18, CXCL13, CCL17, C3, DLL4, APOE, COL4A3, CCL19*	2.76×10^{-5}
G-protein–coupled receptor binding	4	*CCL18, CXCL13, CCL17, CCL19*	1.57×10^{-5}
Chemokine receptor binding	4	*CCL18, CXCL13, CCL17, CCL19*	6.97×10^{-6}
Chemokine activity	4	*CCL18, CXCL13, CCL17, CCL19*	6.37×10^{-6}
Extracellular region	11	*CCL18, COL4A4, CXCL13, CCL17, C3, WNT5B, MMP9, COL4A3, APOE, SPOCK2, CCL19*	7.97×10^{-5}
Extracellular region part	9	*CCL18, COL4A4, CXCL13, CCL17, SPOCK2, APOE, COL4A3, MMP9, CCL19*	7.33×10^{-5}
Sheet-forming collagen	2	*COL4A4, COL4A3*	1.70×10^{-4}
Collagen type IV	2	*COL4A4, COL4A3*	1.21×10^{-4}
KEGG pathway			
γδTCL			
Natural killer cell–mediated cytotoxicity	5	*FCGR3A, KIR3DL1, KLRC2, KLRD1, NCR1*	8.10×10^{-4}
Antigen processing and presentation	4	*KIR3DL1, KLRC2, KLRD1, KLRC4*	7.53×10^{-4}
Atrazine degradation	2	*APOBEC3A, APOBEC3B*	4.42×10^{-4}
αβTCL			
Cytokine–cytokine receptor interaction	5	*CXCL13, CCL17, CCL18, CCL19, TNFRSF25*	2.65×10^{-4}

T cells partially share a cytotoxic immunophenotype with cytotoxic αβ T cells.[1,2] Among 30 patients for whom survival data were available, the prognosis for 8 cases with a γδTCL gene profile (7 γδTCLs and 1 hepatosplenic αβTCL) was not significantly poorer than that of 22 patients with an αβTCL gene profile ($P = .152$; Figure S1). The unusual case of thyroidal γδTCL in the γδTCL gene profile group may affect the result because the *P* value was .009 when we excluded this patient from the survival analysis (data not shown). Future analyses will probably reveal the relationship between our TCR signature gene set and prognostic indicators.

In γδTCL, genes of natural killer (NK) cell–associated molecules, such as killer cell immunoglobulin (Ig)–like receptor (KIR) genes (*KIR3DL1*, *KIR2DL4*, and *KIR2DL2*), and killer cell lectin-like receptors (*KLRC4*, *KLRD1*, and *KLRC2*) were found to be overexpressed (Figure 1; Table S2). These NK receptors are expressed by a subset of NK cells, γδ T cells, and $CD8^+$ αβ T cells.[25] KIR3DL1 and KIR2DL2 exhibit inhibitory functions, and KIR2DL4 has potentially both inhibitory and activating roles.[25] KIR3DL1, KIR2DL2, and KLRD1 are reported to be expressed in some cases of hepatosplenic γδTCL.[26,27] Although *KLRC4*, a top 10 feature gene that characterizes γδTCL and its protein, NKG2F, is expressed in human NK cells,[28] its expression in normal γδ T cells has not been determined. CD16 is also frequently expressed in cases of hepatosplenic γδTCL,[4,27] and its genes (*FCGR3B* and *FCGR3A*) were among the γδTCL signature genes identified in this study.

To search for functionally important genes overexpressed in γδTCL, we performed GO and pathway analysis using 139 of 204 and 53 of 87 known genes in the γδTCL and αβTCL groups, respectively. By WebGestalt, 5 and 20 GO categories were enriched in γδTCL and αβTCL, respectively (Table 1). The enriched GO categories in γδTCL were cellular defense response, signal transduction activity, receptor activity, transmembrane receptor activity, and IgG binding. Three γδTCL pathways and 1 αβTCL pathway were found to be altered in KEGG-signaling analyses (Table 1). No γδTCL and αβTCL signature genes were

shared in a GO category or KEGG pathway, indicating different functional profiles between γδTCL and αβTCL. Four of the 5 γδTCL-enriched GO categories and 2 of the 3 KEGG-signaling pathways altered in γδTCL contained genes encoding KIRs and killer cell lectin-like receptors, a finding that suggests that the expression of these genes may be important for the differential diagnosis of γδTCL and αβTCL.

In conclusion, our current gene expression data confirm that hepatosplenic γδTCL is a distinct lymphoma entity in PTCLs and reveal differences in the gene expression profiles of αβTCL and γδTCL. Further investigations of our newly identified TCR signature genes are warranted to identify novel therapeutic targets and facilitate the diagnosis of γδTCL.

Acknowledgments

We thank the following institutions for providing patient data: Suzuka Chuo General Hospital, Suzuka Kaisei Hospital, Mie University Hospital, Takeuchi Hospital, Tohyama Hospital, Nagai Hospital, Matsusaka Municipal Hospital, Matsusaka Chuo General Hospital, Matsusaka Saiseikai General Hospital, Yamada Red Cross Hospital, and Ise City General Hospital.

This work was supported in part by the Grants-in-Aid for Cancer Research (19-8, 17S-1, 20S-1) from the Ministry of Health, Labor and Welfare, Japan.

Authorship

Contribution: K.M. and M. Yamaguchi designed and performed the study, collected data and samples, interpreted data, and wrote the paper; H.I. and S.T. performed the study and collected samples; M. Yuda and H.S. contributed analytical tools and supervised the research; K.N. collected samples and wrote the paper; and T.K. and N.K. supervised the research and wrote the paper.

Conflict-of-interest disclosure: The authors declare no competing financial interests.

Correspondence: Motoko Yamaguchi, Department of Hematology and Oncology, Mie University Graduate School of Medicine, 2-174 Edobashi, Tsu, Mie 514-8507, Japan; e-mail: waniwani@clin.medic.mie-u.ac.jp.

References

1. Hayday AC. γδ cells: a right time and a right place for a conserved third way of protection. Annu Rev Immunol. 2000;18:975-1026.
2. Carding SR, Egan PJ. γδ T cells: functional plasticity and heterogeneity. Nat Rev Immunol. 2002; 2:336-345.
3. Farcet JP, Gaulard P, Marolleau JP, et al. Hepatosplenic T-cell lymphoma: sinusal/sinusoidal localization of malignant cells expressing the T-cell receptor γδ. Blood. 1990;75:2213-2219.
4. Vega F, Medeiros LJ, Gaulard P. Hepatosplenic and other γδ T-cell lymphomas. Am J Clin Pathol. 2007;127:869-880.
5. Macon WR, Levy NB, Kurtin PJ, et al. Hepatosplenic αβ T-cell lymphomas: a report of 14 cases and comparison with hepatosplenic γδ T-cell lymphomas. Am J Surg Pathol. 2001;25:285-296.
6. Jaffe ES, Harris NL, Stein H, Vardiman JW. World Health Organization Classification of Tumours: Pathology and Genetics of Tumours of Haematopoietic and Lymphoid Tissues. Lyon, France: International Agency for Research on Cancer; 2001.
7. Arnulf B, Copie-Bergman C, Delfau-Larue MH, et al. Nonhepatosplenic γδ T-cell lymphoma: a subset of cytotoxic lymphomas with mucosal or skin localization. Blood. 1998;91:1723-1731.
8. Yamaguchi M, Ohno T, Kita K. γ/δ T-cell lymphoma of the thyroid gland. N Engl J Med. 1997; 336:1391-1392.
9. Yamaguchi M, Ohno T, Nakamine H, et al. γδ T-cell lymphoma: a clinicopathologic study of 6 cases including extrahepatosplenic type. Int J Hematol. 1999;69:186-195.
10. Jaffe ES. Pathobiology of peripheral T-cell lymphomas. Hematology. 2006:317-322.
11. Toro JR, Liewehr DJ, Pabby N, et al. Gamma-delta T-cell phenotype is associated with significantly decreased survival in cutaneous T-cell lymphoma. Blood. 2003;101:3407-3412.
12. Willemze R, Jansen PM, Cerroni L, et al. Subcutaneous panniculitis-like T-cell lymphoma: definition, classification, and prognostic factors: an EORTC Cutaneous Lymphoma Group Study of 83 cases. Blood. 2008;111:838-845.
13. Swerdlow SH, Campo E, Harris NL, et al. WHO Classification of Tumours of Haematopoietic and Lymphoid Tissues. Lyon, France: International Agency for Research on Cancer; 2008.
14. Ballester B, Ramuz O, Gisselbrecht C, et al. Gene expression profiling identifies molecular subgroups among nodal peripheral T-cell lymphomas. Oncogene. 2006;25:1560-1570.
15. Cuadros M, Dave SS, Jaffe ES, et al. Identification of a proliferation signature related to survival in nodal peripheral T-cell lymphomas. J Clin Oncol. 2007;25:3321-3329.
16. de Leval L, Rickman DS, Thielen C, et al. The gene expression profile of nodal peripheral T-cell lymphoma demonstrates a molecular link between angioimmunoblastic T-cell lymphoma (AITL) and follicular helper T (T_{FH}) cells. Blood. 2007;109:4952-4963.
17. Piccaluga PP, Agostinelli C, Califano A, et al. Gene expression analysis of peripheral T cell lymphoma, unspecified, reveals distinct profiles and new potential therapeutic targets. J Clin Invest. 2007;117:823-834.
18. Miyazaki K, Yamaguchi M, Suguro M, et al. Gene expression profiling of diffuse large B-cell lymphoma supervised by CD21 expression. Br J Haematol. 2008;142:562-570.
19. National Center for Biotechnology Information. GEO: Gene Expression Omnibus. http://www.ncbi.nlm.nih.gov/geo/. Accessed July 1, 2008.
20. Zhang B, Kirov S, Snoddy J. WebGestalt: an integrated system for exploring gene sets in various biological contexts. Nucleic Acids Res. 2005;33: W741-W748.
21. Vanderbilt University. WebGestalt. http://bioinfo.vanderbilt.edu/webgestalt/. Accessed May 2, 2008.
22. Kanehisa M, Goto S. KEGG: Kyoto encyclopedia of genes and genomes. Nucleic Acids Res. 2000; 28:27-30.
23. Kanehisa Laboratories. KEGG: Kyoto Encyclopedia of Genes and Genomes. http://www.genome.ad.jp/kegg/. Accessed May 2, 2008.
24. Staudt LM, Dave S. The biology of human lymphoid malignancies revealed by gene expression profiling. Adv Immunol. 2005;87:163-208.
25. Lanier LL. NK cell recognition. Annu Rev Immunol. 2005;23:225-274.
26. Haedicke W, Ho FC, Chott A, et al. Expression of CD94/NKG2A and killer immunoglobulin-like receptors in NK cells and a subset of extranodal cytotoxic T-cell lymphomas. Blood. 2000;95: 3628-3630.
27. Morice WG, Macon WR, Dogan A, Hanson CA, Kurtin PJ. NK-cell-associated receptor expression in hepatosplenic T-cell lymphoma, insights into pathogenesis. Leukemia. 2006;20:883-886.
28. Kim DK, Kabat J, Borrego F, Sanni TB, You CH, Coligan JE. Human NKG2F is expressed and can associate with DAP12. Mol Immunol. 2004;41: 53-62.

Molecular Microbiology (2010) 75(4), 854–863 ■

doi:10.1111/j.1365-2958.2009.07005.x
First published online 27 January 2010

Transcription factor AP2-Sp and its target genes in malarial sporozoites

Masao Yuda,[1]* Shiroh Iwanaga,[1] Shuji Shigenobu,[2] Tomomi Kato[1] and Izumi Kaneko[1]

[1]*Department of Medical Zoology, Mie University School of Medicine, Mie, Tsu, 514-0001, Japan.*

[2]*Okazaki Institute for Integrative Bioscience, National Institute for Basic Biology, National Institutes of Natural Sciences, Higashiyama, Myodaiji, Okazaki, Japan.*

Summary

The malarial sporozoite is the stage that infects the liver, and genes expressed in this stage are potential targets for vaccine development. Here, we demonstrate that specific gene expression in this stage is regulated by an AP2-related transcription factor, designated AP2-Sp (APETALA2 in sporozoites), that is expressed from the late oocyst to the salivary gland sporozoite. Disruption of the AP2-Sp gene did not affect parasite replication in the erythrocyte but resulted in loss of sporozoite formation. The electrophoretic mobility-shift assay showed that the DNA-binding domain of AP2-Sp recognizes specific eight-base sequences, beginning with TGCATG, which are present in the proximal promoter region of all known sporozoite-specific genes. Promoter assays demonstrated that these sequences act as *cis*-acting elements and are critical for the expression of sporozoite-specific genes with different expression profiles. In transgenic parasites that express endogenous AP2-O (APETALA2 in ookinetes), but whose AP2 domain had been swapped with that of AP2-Sp, several target genes of AP2-Sp were induced in the ookinete stage. These results indicate that AP2-Sp is a major transcription factor that regulates gene expression in the sporozoite stage.

Introduction

During a complex life cycle, *Plasmodium* parasites invade different types of host cell and significantly change gene expression in each stage. Until recently, however, the mechanisms of stage-specific gene regulation remained unclear and transcription factors (TFs) participating in this regulation were unknown.

Recently, Apetala2 (AP2) family genes were identified in *Plasmodium* species and were suggested to encode *Plasmodium* sequence-specific TFs (Balaji *et al.*, 2005). This family is characterized by the AP2 domain, a DNA-binding domain composed of approximately 60 amino acids that was first identified in *Arabidopsis* APETALA2 protein (Jofuku *et al.*, 1994). In human and rodent *Plasmodium* parasites, this family is composed of 26 members, and the amino acid sequences of the AP2 domains are highly conserved among orthologues.

AP2-related genes have been reported to be expressed in asexual intra-erythrocytic stages of *Plasmodium* parasites. In *Plasmodium falciparum* their expression during asexual replication is co-ordinated with cell cycle progression (Balaji *et al.*, 2005; De Silva *et al.*, 2008). Among these AP2-related genes two (PlasmoDB identifier: PF14_0633 and PFF0200c) have been suggested to participate in the induction of a group of genes that are required in a cell cycle-specific manner (De Silva *et al.*, 2008). In a previous paper we reported that an AP2 family protein, designated AP2-O (Apetala2 in ookinetes), regulates stage-specific gene expression in the ookinete, which is a motile stage that invades the mosquito midgut (Yuda *et al.*, 2009). AP2-O has a single AP2 domain and binds to the proximal promoter region of target genes with this domain, thereby inducing several genes involved in mosquito midgut-invasion. These findings indicate that AP2-related TFs are widely used for gene regulation in the *Plasmodium* life cycle.

The *Plasmodium* sporozoite is the stage that infects the mammalian liver. Genes expressed in this stage are potential targets for vaccine development. Identification of TFs and elucidation of the mechanisms of gene regulation in this stage should yield novel means to discover vaccine antigens. Here, we show that an AP2-related protein, designated AP2-Sp (AP2 in sporozoites), plays a central role in gene expression in the sporozoite stage using the rodent malaria parasite *Plasmodium berghei*. We also show that AP2-Sp is not necessary for parasite

Accepted 30 November, 2009. *For correspondence. E-mail m-yuda@doc.medic.mie-u.ac.jp; Tel. (+81) 59 231 5430; Fax (+81) 59 231 5430.